mathematics

MDPI

Article

Gait Dynamics Classification with Criticality Analysis and Support Vector Machines

Shadi Eltanani [1,*], Tjeerd V. olde Scheper [1], Johnny Collett [2], Helen Dawes [3] and Patrick Esser [2]

[1] School of Engineering, Computing and Mathematics, Faculty of Health, Science and Technology, Oxford Brookes University, Headington Hill Campus, Headington, Oxford OX3 0BP, UK; tvolde-scheper@brookes.ac.uk
[2] Faculty of Health and Life Sciences, Oxford Brookes University, Headington Campus, Headington, Oxford OX3 0BP, UK; jcollett@brookes.ac.uk (J.C.); pesser@brookes.ac.uk (P.E.)
[3] NIHR Exeter BRC, Medical School, University of Exeter, St Luke's Campus, Exeter EX1 2LU, UK; h.dawes@exeter.ac.uk
* Correspondence: seltanani@brookes.ac.uk

Abstract

Classifying demographic groups of humans from gait patterns is desirable from several long-standing diagnostic and monitoring perspectives. IMU recorded gait patterns are mapped into a nonlinear dynamic representation space using criticality analysis and subsequently classified using standard Support Vector Machines. Inertial-only gait recordings were found to readily classify in the CA representations. Accuracies across age categories for female versus male were 72.77%, 78.95%, and 80.11% for $\sigma = 0.1$, 1, and 10, respectively; within the female group, accuracies were 73.36%, 76.70%, and 78.90%; and within the male group, 77.65%, 81.48%, and 81.05%. These results show that dynamic biological data are easily classifiable when projected into the nonlinear space, while classifying the data without this is not nearly as effective.

Keywords: criticality analysis; support vector machine; gait pattern detection; chaotic mathematical model; rate control of chaos; demographic analysis

MSC: 37M22; 93C15; 34H10

1. Introduction

Dynamic modelling methods for interpreting biological signals such as gait have become increasingly important in various applications that include human activity recognition [1], clinical diagnosis [2], rehabilitation monitoring [3], and security surveillance [4]. Despite their widespread use, traditional methods often fall short in extracting the complex dynamics of human movement, which prevents the precise detection and classification of gait patterns, particularly when dealing with large datasets [5]. These limitations require the integration of advanced machine learning and signal processing techniques to achieve the desired level of detail and accuracy [6]. Gait dynamics are fundamentally complex and nonlinear, characterised by obvious variations across populations. Criticality Analysis (CA), which is based on a method to control chaos, provides a promising solution to greatly enhance gait analysis performance [7]. This approach stabilises system dynamics and enables the detection of discrepancies and visualisation of dynamic trajectories in a data-agnostic manner. The CA uses a biologically inspired chaotic mathematical model with Rate Control of Chaos to control exponential growth and restore stability to systems

Academic Editors: Guillermo Huerta-Cuellar, Jesus M. Munoz-Pacheco and José Luis Echenausía-Monroy

Received: 20 October 2025
Revised: 18 December 2025
Accepted: 30 December 2025
Published: 2 January 2026

perturbed by external factors. A network of these RCC oscillators results in a Self-Organised Critical System [8] that responds to nonlinear external perturbations. Representing gait patterns using this method allows for a more precise identification of anomalies and improved assessment of gait stability. Such capabilities are essential for accurate gait analysis, including early detection of gait-related diseases and the monitoring of rehabilitation progress. However, the CA method produces periodic dynamics from the gait pattern and SVMs provide a classification framework well suited to this type of representation. These two complementary methods transform high-dimensional, complex, nonlinear data into a lower-dimensional space for easier classification. The Gaussian kernel function within SVMs assists in identifying these complex structures in gait data, which makes SVMs a suitable candidate for the classification of CA representations of data [9,10].

The main contribution of this work demonstrates that the CA method can help detect and understand gait dynamics across different demographic groups, which is not readily feasible using the raw IMU data alone. We apply the CA model to three groups from the Science Museum dataset and map their movement patterns in phase space. We then use an SVM classifier to support the evaluation, which shows that the CA method makes the gait patterns clearer and easier to distinguish. Our results indicate that the combined CA and SVM approach reveals important nonlinear features in the data and can be useful for future gait analysis in clinical and rehabilitation settings.

The paper is structured as follows: Section 2 reviews the current literature, introduces nonlinear dynamic modelling and the criticality analysis method, and highlights the main contributions of this study. Section 3 presents the fundamentals of dynamic systems. Section 4 introduces the topology of the phase space associated with the CA methodology and describes how the system dynamics may be captured through a reduced set of state variables. Section 5 develops the mathematical framework for criticality analysis of human gait. Section 6 describes the gait model, details the experimental setup, and presents the results with a discussion of their implications. Finally, Section 7 concludes the paper.

2. Related Work

This section reviews the key studies in gait recognition and sets out the gaps that motivated our criticality analysis approach.

2.1. Criticality Analysis for Human Gait

Recently, there has been an increasing interest in studying human gait patterns, particularly in the applications of biomechanics, robotics, and healthcare [11]. The complexity and dynamic nature of gait have led to the use of nonlinear chaotic mathematical models to better understand its complexities. Initial efforts focused on developing mathematical models that use control functions to generate optimal walking trajectories, which help individuals walk with minimal muscle effort while maintaining balance and control [12]. These models were extended to explore the nonlinear aspects of walking performance through a passive compass gait model [13]. Although simple, this model revealed both regular and chaotic behaviours, highlighting the intricate nature of gait dynamics. Building on these insights, practical applications based on mathematical models emerged, such as the development of cylindrical electromagnetic vibration harvesters [14]. These devices measure the mechanical energy generated from human gait and convert it into electrical energy, powering small biomedical implants without needing external batteries or recharging. The vibrations produced by these harvesters during walking provide crucial information about their performance across various walking speeds and gait conditions, demonstrating the practical impact of understanding gait dynamics. To address the complexities revealed by these applications, chaotic control principles were applied. Techniques such as the

bifurcation method, combined with artificial neural networks, were used to manage unpredictability and restore stability within chaotic gait patterns [15]. Additionally, models linking gait dynamics to the nervous system were developed by incorporating external stimuli into a fractional diffusion equation. This approach provided a more comprehensive view into how external factors and neural control interact to influence walking patterns, leading to more precise predictions of gait patterns. Furthermore, studies have examined how gait varies in younger and older adults during spontaneous walking and treadmill walking [16]. These studies, using nonlinear dynamics, found that older adults show greater variability in their gait, suggesting that aging affects walking stability. Moreover, integrating chaos theory into nonlinear dynamics models has shed light on the complex interactions between neural control, biomechanics, and environmental factors [17]. This approach has been particularly effective in studying long-range correlations in stride intervals associated with pathological gait patterns [18,19]. While these methods differ from the one used in this paper, the findings theoretically reinforce the idea that nonlinear approaches provide more thorough gait analysis than traditional linear methods [20].

Furthermore, studies have examined how gait varies across different populations, highlighting the influence of age and gender on gait variability.

2.2. Age-Dependent Changes in Gait Variability

Gait speed decline is generally associated with increasing age [21,22], along with increases in gait parameter variability, such as step width, stepping distance, and stepping rate [23]. Whilst the exact mechanisms are complex, increased variability is often linked to age-related muscular stiffness and weakness, which challenge dynamic balance control and elevate the risk of falls [24]. Individuals with higher relative muscle performance, often associated with increased physical activity, demonstrate reduced variability within their gender's gait patterns [25]. From a gait perspective, the most significant physiological contributor to increased variance occurs during toe-off and the transition from double-to-single stance, which relies on complex anteroposterior and mediolateral dynamic stability [26].

2.3. Gender Differences in Gait Variability

Irrespective of walking speed, females commonly exhibit larger dynamic gait variability [27], particularly during the early swing-phase, when bodyweight shifts ahead of the ipsilateral forefoot in the anterior–posterior direction. Some studies also report increased medio-lateral gait variance [28], which correlates with the most common fall directions [29]. Despite these observations, there is no clear physiological explanation for the higher degree of gait variability in females, although it has been consistently observed in both healthy and clinical populations [30,31].

2.4. State of the Art and Main Contributions

Previous research has utilised a nonlinear chaotic mathematical model with a control function designed to control nonlinear growth in dynamic systems and restore stability. This was achieved by introducing a control term into the influencing nonlinear variables, based on the concept of Rate Control of Chaos (RCC) [7]. The model was subsequently applied to two real-world datasets to detect abnormalities in gait patterns, with these patterns being quantified and classified using supervised machine learning techniques, such as the SVM classifier, with high accuracy [9,10].

To the best of our knowledge, this paper makes a unique contribution by applying this approach to a new real-world dataset, as described in Section 6.1. This approach generates scale-free and nonlinear data representations in a low-dimensional manifold, which enables the precise detection of complexities in human gait and helps distinguish specific age–gait patterns. The output of the CA model is then used as input features for a support vector

machine (SVM) classifier, which utilises a Gaussian kernel function to enhance overall detection accuracy.

3. Overview of Dynamic Systems

Dynamical systems modelling has a long history in mathematical biology, where it has helped scientists explain processes that evolve over time, from the scale of single molecules to entire populations [32]. At the level of individual cells, the same modelling tools are used to describe metabolism, signalling, and the way biological components interact as networks whose states continuously change.

When we shift from cells to whole-body motion, the logic is similar. Human walking is not random muscle activity, but a coordinated rhythm built from many interacting muscle groups. Because of that rhythm, models based on coupled oscillators are a natural fit for representing gait, where each oscillator carries the signal of one muscle or functional muscle unit. What matters most in these models is not only the strength of each signal, but the timing between them, whose phase relationships shape smooth and efficient movement [33].

Gait also adapts. The same walking pattern a person uses on flat ground may change with speed, slope, surface type, or sudden disturbances such as a push or change in balance. Dynamical systems models allow these changes to be studied mathematically, especially how far a walking rhythm can shift before losing stability, and how quickly it can recover or reorganise itself under new conditions [34,35].

Beyond modelling itself, dynamical systems theory provides data analysis tools that describe how predictable or variable a walking signal is over time. Measures such as phase reconstruction, attractors, and Lyapunov exponents help quantify the internal dynamics of gait trajectories, including how stable they remain, and how widely they spread when conditions or participants change [36,37]. Practically, the same mathematical language used to understand cellular networks can also be used to understand the organisation and resilience of human walking.

A dynamical system can be written as ordinary differential equations (ODEs) whose state updates forward in time, either continuously or at discrete time steps. The system is deterministic if the current state fixes exactly one future state, whereas a stochastic system moves toward a range of future states governed by probability. Chaos theory sits in the deterministic world, focusing on systems whose trajectories can shift dramatically when their starting points shift even by a tiny amount [38].

Deterministic chaotic systems are commonly expressed in ODE form:

$$\begin{aligned} \frac{dx^{(1)}}{dt} &= F_1\left(x^{(1)}, x^{(2)}, x^{(3)}, \ldots, x^{(N)}\right), \\ \frac{dx^{(2)}}{dt} &= F_2\left(x^{(1)}, x^{(2)}, x^{(3)}, \ldots, x^{(N)}\right), \\ &\vdots \\ \frac{dx^{(N)}}{dt} &= F_N\left(x^{(1)}, x^{(2)}, x^{(3)}, \ldots, x^{(N)}\right). \end{aligned} \tag{1}$$

or more compactly as

$$\frac{d\mathbf{x}(t)}{dt} = \mathbf{F}(\mathbf{x}(t)), \tag{2}$$

where $\mathbf{x}(t)$ represents the full system state as an N-dimensional vector. Once the system is initialised at $\mathbf{x}(0)$, its trajectory $\mathbf{x}(t)$ for later time points ($t > 0$) is fully determined by the functions inside $\mathbf{F}$.

The transition of the system through stability, oscillation, or chaos depends on how $\mathbf{F}$ behaves when it reaches $\mathbf{F}(\mathbf{x}(t)) = \mathbf{0}$, whose condition defines equilibrium points. A fixed solution that satisfies this condition means the system is stable and unchanging at that point [39,40]. If the system repeats its path over time after a period T, so that $\mathbf{x}(t) = \mathbf{x}(t + nT)$ for $n \in \mathbb{Z}$, it forms a periodic orbit or cycle.

Chaotic behaviour appears when the system is not fixed, nor repeating, but constantly changing within phase space, never settling into one point or one cycle. In that regime, even a small disturbance at $\mathbf{x}(0)$ can shift future states enough that two nearly identical starting points eventually drift apart into very different trajectories [41]. That sensitivity is not a modelling flaw; it is often the signature that the system contains rich but tightly coupled internal dynamics.

4. Topology of Phase Space

The phase space manifold represents the full set of possible states a dynamical system can occupy. In a deterministic system, knowing the current state, and sometimes the previous states, allows for the prediction of future states. In practice, however, the governing equations can be highly complex, making direct interpretation challenging for applications like human gait analysis. Despite this complexity, the structure of the phase space holds essential information about the system's dynamics. Mathematically, the state of the system at any time t can be expressed as follows:

$$\mathbf{x}(t) = \left(x^{(1)}, x^{(2)}, x^{(3)}, \ldots, x^{(N)}\right). \tag{3}$$

For the extended model applied to gait dynamics, the phase space can be simplified to focus on key variables of interest. In this case, the system state is described by

$$\mathbf{x}(t) = (F, M), \tag{4}$$

where F and M capture the dominant features of the gait pattern in the phase plane. This projection makes it possible to visualise and analyse the underlying dynamics even in a high-dimensional system.

5. Mathematical Model for Criticality Analysis of Human Gait

The criticality analysis method [8], described in (5)–(11), is a nonlinear dynamical system defined by a set of time derivatives that govern the interaction between two biochemical components. The extracellular matrix, m, forms from soluble filaments, f, through a process mediated by the transglutaminase enzyme, g, which reassembles filaments into the matrix. At the same time, the proteinase enzyme, p, breaks down the matrix m back into filaments f. This interplay between deconstruction and reassembly maintains a dynamic balance, ensuring proper regulation of both m and f [42].

The Rate Control of Chaos (RCC), as defined in (8)–(11), describes how the system variables evolve over time, particularly the production rates of enzymes p and g. The filament concentration, f, plays a key nonlinear role in the system. RCC modulates this effect using the function in (5), limiting deviations and stabilising the system. By tuning the parameters of this control function, it is possible to adjust the degree of control over the chaotic dynamics [7]. The bifurcation parameter, r_{im}, serves as an external perturbation, providing a steady input that drives matrix production.

As the system evolves, it exhibits rich nonlinear phenomena such as bistability, limit cycles, spirals, and chaos, especially near critical transitions. Its states are represented in an n-dimensional phase space manifold, which captures nonlinear correlations, the interactions of coupled dynamics, and the scale-invariant nature of critical fluctuations. In the

model (5)–(11), the trajectories of f and m correspond to the scale-free nonlinear response of the system when perturbed by r_{im}.

While the Berry model [8,42] is inspired by subcellular processes rather than gait directly, it can be applied to human walking by highlighting critical transitions in biological systems. It is important to emphasise that the nonlinear representation resulting from the mapping into the network of oscillators is based on the Self-Organised Critical state of each of those oscillators. This means that the system is sensitive to small perturbations and assume different orbits depending on those perturbations. Furthermore, the RCC control ensures that the system remains stable and in a weak chaotic state that enables the SOC to emerge. The parameter space formed by the network of individually controlled oscillators is conveniently less relevant to the results, as any RCC-controlled network of oscillators is capable of producing these mappings, without loss of generality [8]. The method, therefore, allows for the detection of subtle gait instabilities that may be overlooked by conventional or direct methods. In this context, the model reflects how muscles, joints, and the nervous system coordinate to adapt to varying conditions. Efficient gait control relies on continuous feedback from sensory receptors (afferent signals) and motor responses (efferent signals), regulating muscle activity and maintaining neuromuscular coordination. External forces generated during walking, combined with internal energy expenditure to drive muscle function and modulate neurotransmitters, are all captured in the dynamics of this control framework.

$$q_f = \frac{f}{f + \mu_f}, \tag{5}$$

$$\sigma_p(q_f) = f_p e^{(x_p q_f)}, \tag{6}$$

$$\sigma_g(q_f) = f_g e^{(x_g q_f)}, \tag{7}$$

$$\frac{dm}{dt} = k_g \frac{fg}{K_G + f} - \frac{mp}{1 + m} + r_{im}, \tag{8}$$

$$\frac{df}{dt} = -k_g \frac{fg}{K_G + f} + \frac{mp}{1 + m} - \frac{fp}{1 + f}, \tag{9}$$

$$\frac{dp}{dt} = \sigma_p(q_f)\gamma \frac{f^n}{K_R^n + f^n} - k_a p^2, \tag{10}$$

$$\frac{dg}{dt} = \sigma_g(q_f)\beta \frac{f^l}{K_S^l + f^l} - k_{deg} \frac{gp}{K_{deg} + g}. \tag{11}$$

The CA mathematical model includes several parameters: $\gamma = 0.026$, $\beta = 0.00075$, $K_R = 4.5$, $K_S = 1$, $K_G = 0.1$, $K_{deg} = 1.1$, $k_g = k_{deg} = 0.05$, and $k_a = \frac{k_{deg}}{K_{deg}} = 0.0455$. The Hill coefficients n and l are both set to four. The bifurcation parameter r_{im} drives a range of dynamic behaviors, including stable periodic cycles, bistability, and chaos, and it is kept constant across all oscillators within the chaotic domain. An external input is applied as a perturbation to r_{im}, as described in (12), linking the oscillators through a relative scale contribution from all other oscillators. The RCC control parameters in (5)–(7) ($f_p = f_g = 1$, $x_p = x_g = -1$, and $\mu_f = 2$) remain fixed throughout the simulation experiments in this study. These parameters, however, can be adjusted to allow individual oscillators to shift their oscillatory trajectories, providing flexibility in controlling local dynamics.

$$r_{im}{}^i = \sum_{j=1, j \neq i}^{n} w_j m_j + \varepsilon. \tag{12}$$

The connectivity strength between oscillators, denoted by w_j, varies across the values 0.00011, 0.00012, and 0.00025. External perturbations, represented by ε, follow a Gaussian distribution and are scaled within the range $[-1, 1]$. These perturbations are applied over multiple evolution steps to examine how they influence the different oscillatory cycles. For the experiments in this paper, a connectivity strength of $w_j = 0.0002$ was empirically chosen from the chaotic domain of the oscillators to investigate its impact on the system's dynamics while preserving overall stability.

$$M = \sum_{i=1}^{n} m_i, \tag{13}$$

$$F = \sum_{i=1}^{n} f_i. \tag{14}$$

The total unweighted dynamics, M and F in (13) and (14), were obtained by summing the contributions of all individual oscillators. This approach allows the overall system behavior to be observed, even when the activity of single oscillators cannot be directly monitored. A network of 16 oscillators was used, and the local dynamics of each oscillator could be adjusted in response to perturbations from neighboring oscillators. The RCC model equations and the generated data can be found in [43].

The original model (8)–(11) was first simulated to examine how RCC control affects stability. Initial conditions were set as $m(0) = f(0) = p(0) = g(0) = 0.8$, and the simulation was conducted over 94×10^5 points with a time step of 0.5.

When RCC control was applied, more structured and stable trajectories were observed, particularly at $\xi_p = -1$, as illustrated in Figure 1. A slight reduction in amplitude was noted compared to the uncontrolled system, but overall stability was improved. Time series plots (Figures 2–5) show consistent oscillations around 9.2561×10^4. For $x_p = -3$, sparser trajectories were recorded on the f–m plane, and stabilisation occurred more slowly, reaching 10.743×10^4. In these simulations, x_p and x_g were set to -1 for stable trajectories and -3 for the sparser ones.

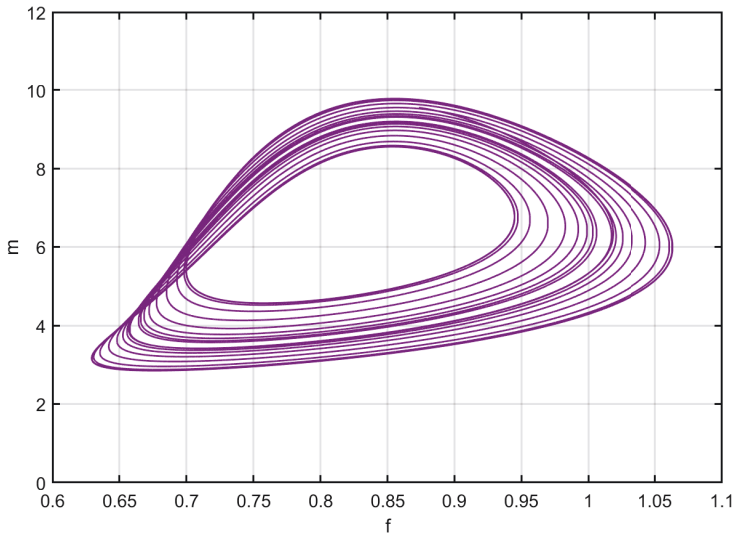

Figure 1. Phase plot projection in the f–m plane, showing the system evolution from one dynamic regime to another. Control is activated at approximately 1×10^4 s. Chaotic oscillations dominate before control, and give way to a clearly stabilised trajectory after control is applied, as seen in Figures 2–5.

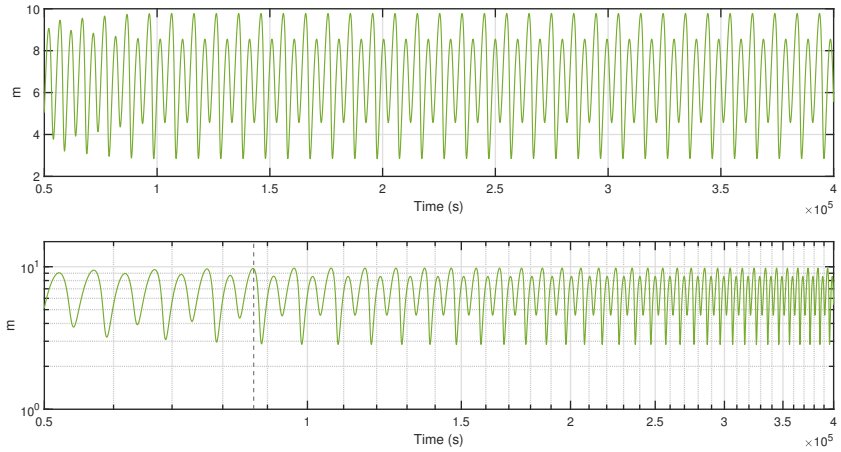

Figure 2. Example output from the chaotic Berry model, with control activated at the dotted line. The top panel plots the modelled variable m over time. The bottom panel shows the same signal on a logarithmic time scale, making changes in growth rate and stability easier to observe before and after control is applied.

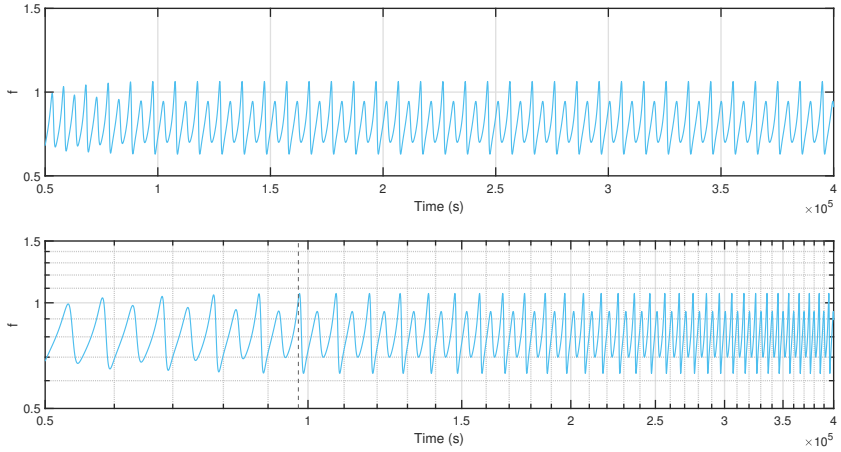

Figure 3. Example output from the chaotic Berry model, with control activated at the dotted line. The top panel plots the modelled variable f over time. The bottom panel shows the same signal on a logarithmic time scale, making changes in growth rate and stability easier to observe before and after control is applied.

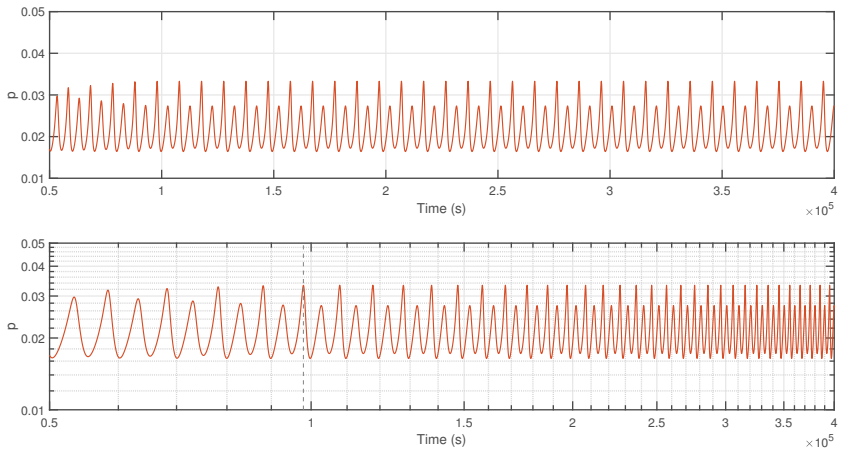

Figure 4. Example output from the chaotic Berry model, with control activated at the dotted line. The top panel plots the modelled variable p over time. The bottom panel shows the same signal on a logarithmic time scale, making changes in growth rate and stability easier to observe before and after control is applied.

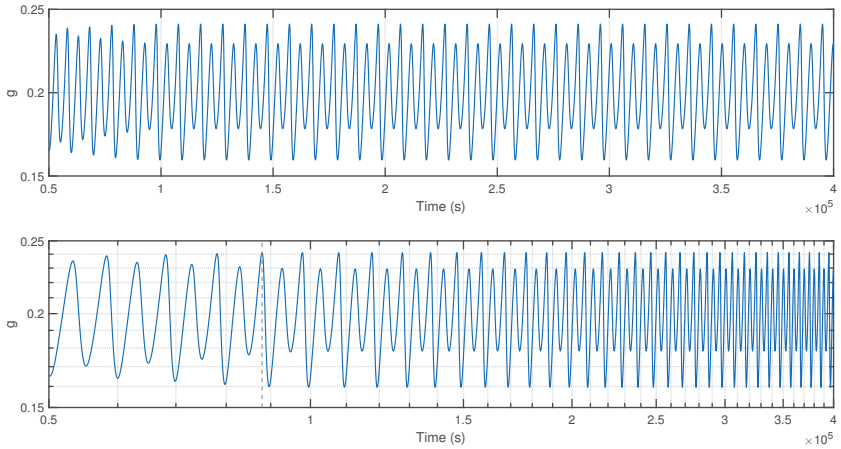

Figure 5. Example output from the chaotic Berry model, with control activated at the dotted line. The top panel plots the modelled variable g over time. The bottom panel shows the same signal on a logarithmic time scale, making changes in growth rate and stability easier to observe before and after control is applied.

Phase-space trajectories in the f–m plane were used to represent the dynamic characteristics of the model and its sensitivity to small perturbations. These manifolds were then supplied as input features for the SVM, which allows the supervised learning algorithm to detect patterns generated by the coupled oscillator network.

6. Methodology

The proposed framework for the CA gait dynamic representation, illustrated in Figure 6, was evaluated using the Science Museum dataset. This framework is designed to classify gait patterns of human based on their age.

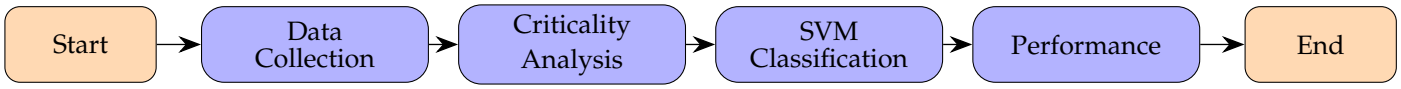

Figure 6. Data processing workflow for CA gait dynamics classification.

6.1. Science Museum Dataset

Individuals aged 5 to 80 were invited to participate in the Live Sciences at the Science Museum in London. Informed consent was obtained in accordance with approvals from the Oxford Brookes University Research Ethics Committee (UREC). Two ethics approvals were applied: UREC number 100490 for participants aged 5–16, and UREC number 090434 for participants aged 16–80. Participant characteristics, including age (years), gender (m/f), self-reported ethnicity, height (m), weight (kg), foot length (based on shoe size), and leg length (measured from the anterior superior iliac spine to the medial malleolus), were recorded. Each participant walked a 10-meter distance at a self-selected speed while wearing an inertial measurement unit placed over the projected center of mass in the lower lumbar region (4th lumbar vertebra). Temporal (step time [ms], cadence [steps/min]) and spatial (step length [m], stride length [m], walking speed [m/s]) gait parameters were derived using validated models based on leg length and foot size [44,45]. The final dataset consisted of 2019 participants, including 1105 females and 914 males. Participants were categorised into five age groups for both genders: Children (2–12 years), Adolescents (13–18 years), Young Adults (19–44 years), Middle-aged Adults (45–64 years), and Older Adults (65+ years).

The Museum dataset, which represents the IMU signals in the x, y, and z axes, was used as is as a perturbing input to the criticality analysis model described above, whose output was standardised (z-score) before being fed into the SVM classifier.

6.2. Experiments and Results

The proposed CA approach was evaluated using the age-based gait patterns from the Museum dataset. The goal of this evaluation is twofold:

(A) To classify the gait patterns of children, adolescents, young adults, middle-aged, and old-aged adults by comparing males and females within each age group, as well as analysing gait patterns across pairwise age group comparisons for a single gender group (male or female).

(B) To examine the robustness of the CA approach in using machine learning models, e.g., the SVM classifier, to differentiate male and female gait patterns.

6.2.1. CA for Age-Based Gait Patterns

The three experiments described in Section 6.2 were established to compare gait patterns of individuals using the CA methodology, as detailed in (5)–(11). The raw data samples in the main dataset corresponding to a specific demographic group have been paired with another age group, either within the same gender or across different genders. In the first experiment, we compared gait patterns for both genders, with datasets denoted as $\{\mathbf{x}_{\text{fm1}} \ldots \mathbf{x}_{\text{fm5}}\}$ for female and male children, adolescents, young adults, middle-aged, and old-aged adults. For the second experiment, we focused on female-specific pairwise age group comparisons, represented by $\{\mathbf{x}_{\text{f1}} \ldots \mathbf{x}_{\text{f10}}\}$ for various combinations of female children, adolescents, young adults, middle-aged, and old-aged adults. In the last experiment, which is identical to the second, we conducted pairwise age group comparisons for males, with datasets denoted as $\{\mathbf{x}_{\text{m1}} \ldots \mathbf{x}_{\text{m10}}\}$, corresponding to male children, adolescents, young adults, middle-aged, and old-aged adults.

We mapped the CA walking data into phase plots, with each line representing the gait force trajectory of one participant. In Figure 7, the left column shows female participants and the right column shows male participants. Rows correspond to the five age groups: children, adolescents, young adults, middle-aged adults, and older adults. The phase plots are drawn between the total gait force components F_{total} and M_{total}, generated through a perturbed 16-oscillator dynamic network. These plots reveal distinct nonlinear domains and clustering behaviour in the model's phase space, showing how gait patterns consistently group according to demographic profiles.

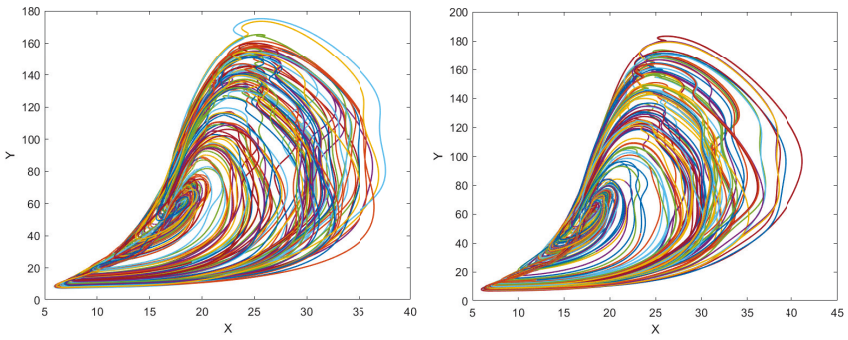

(**a**) Female Child Walk (**b**) Male Child Walk

Figure 7. *Cont.*

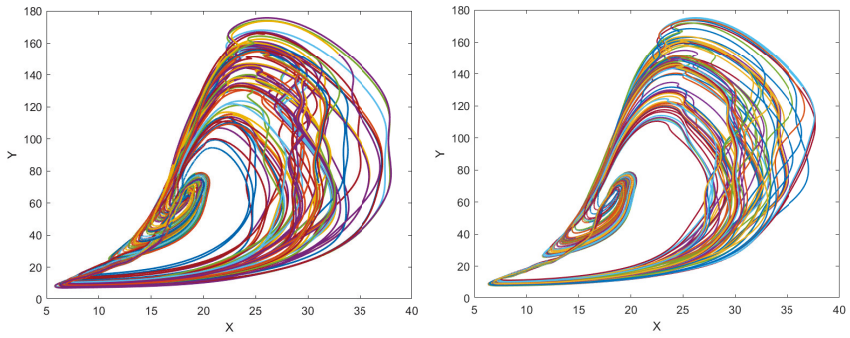

(**c**) Female Adolescents Walk (**d**) Male Adolescents Walk

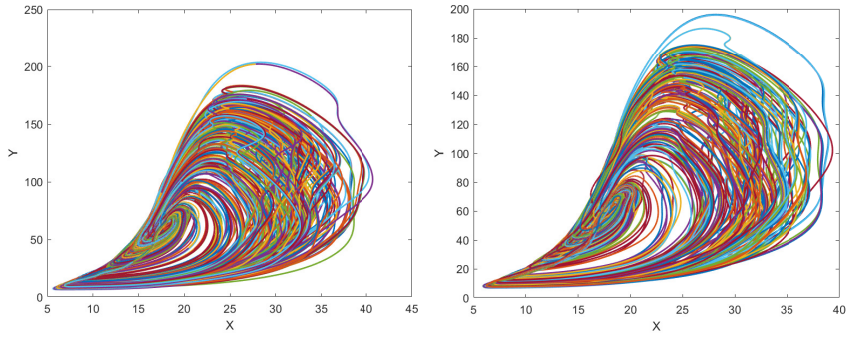

(**e**) Female Young Adults Walk (**f**) Male Young Adults Walk

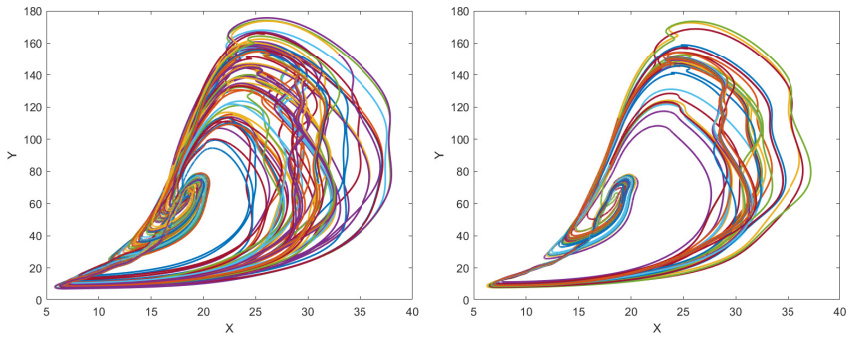

(**g**) Female Middle Aged Walk (**h**) Male Middle Aged Walk

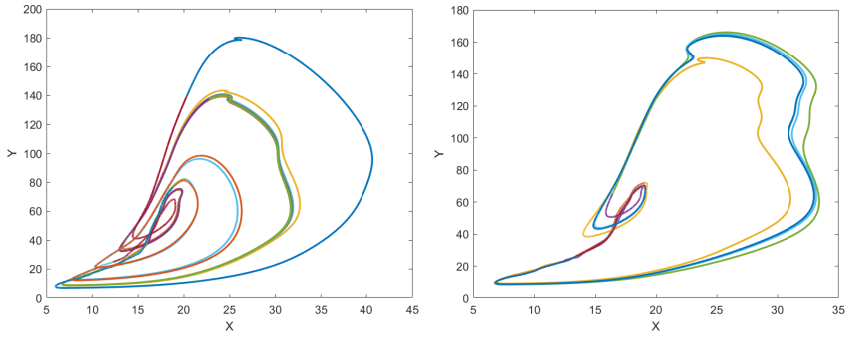

(**i**) Female Old Aged Walk (**j**) Male Old Aged Walk

Figure 7. Phase plots of gait trajectories across demographic groups, with axes representing the interaction between total force projections in the two dynamic domains M (vertical axis) and F (horizontal axis). Each line corresponds to one participant's gait trace. The left column shows female participants and the right column shows male participants. Rows represent children, adolescents, young adults, middle-aged adults, and older adults. The gait signal F_{total} is transformed using a perturbed 16-oscillator dynamic network, showing separate nonlinear decision regions and clustering patterns characteristic of each age and gender group.

The CA methodology not only provides an efficient data representation tool but also serves as a microscopic lens, which reveals stability and differences in gait patterns that may not be immediately apparent through traditional feature analysis alone. Moreover, male children showed more extended trajectories along the Y-axis, indicating greater variability, which could mean larger step lengths or more dynamic movement. This might be linked to factors like muscle mass and energy levels. In contrast, female children's trajectories were more compact, which may indicate cautious movement or reflect early-stage neuromotor control aimed at maintaining stability. Among young adults, there was a noticeable shift to more consistent walking patterns. Female young adults showed more efficient, goal-driven movement, while male young adults covered a larger spatial area, likely due to longer stride lengths and faster walking speeds, which are influenced by muscle mass and physical activity levels. For elderly individuals, both males and females exhibited more compact trajectories, suggesting an emphasis on stability and cautious movement. Female elderly individuals showed more constrained movement patterns, likely prioritising balance, while male elderly individuals maintained slightly broader trajectories, which could be due to attempts to preserve stride length. These differences reflect typical age-related changes in muscle strength, joint flexibility, and the potential influence of psychological factors such as confidence and fear of falling.

6.2.2. SVM for Age-Related Gait Patterns

The phase plots shown in Figure 7 make it straightforward to differentiate walking patterns across various demographic groups. However, machine learning algorithms could be utilised to quantify these distinctive features generated by the CA phase plots, which enable accurate age prediction through gait pattern analysis. Particularly, the CA input features were then used as inputs to the SVM classifier. The SVM classifier uses a Gaussian kernel function due to its ability to map the CA nonlinear representation into a higher-dimensional space, making nonlinear complex patterns more separable. Details of the technical implementation of the SVM classifier can be found in [9,10].

Figure 8 shows the decision boundaries generated by SVM models using a Gaussian kernel to classify the gait patterns of different demographic groups. It compares males and females within each age group, with varying regularisation parameters $C = 0.1$, $C = 1$, and $C = 10$. As C increases, the decision boundary becomes more complex, shifting from a smooth generalised line as in Figure 8a, to a more tightly fitting boundary around the data points as in Figure 8c. This indicates the increased sensitivity of the model to correctly classify data points at the expense of potentially overfitting, a typical behavior observed when adjusting the regularisation parameter in SVMs. The variance in decision boundaries suggests that higher C values allow for more flexibility but risk capturing noise as part of the pattern, especially in the presence of overlapping class distributions.

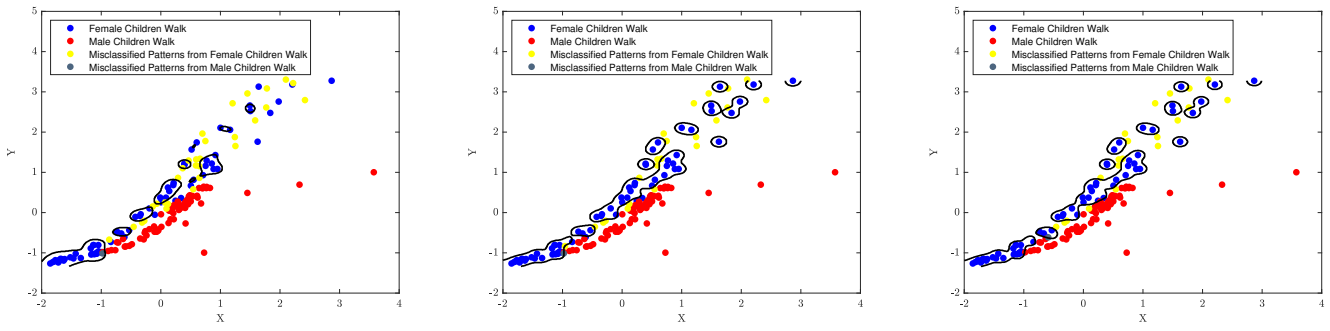

(**a**) (**b**) (**c**)

Figure 8. *Cont.*

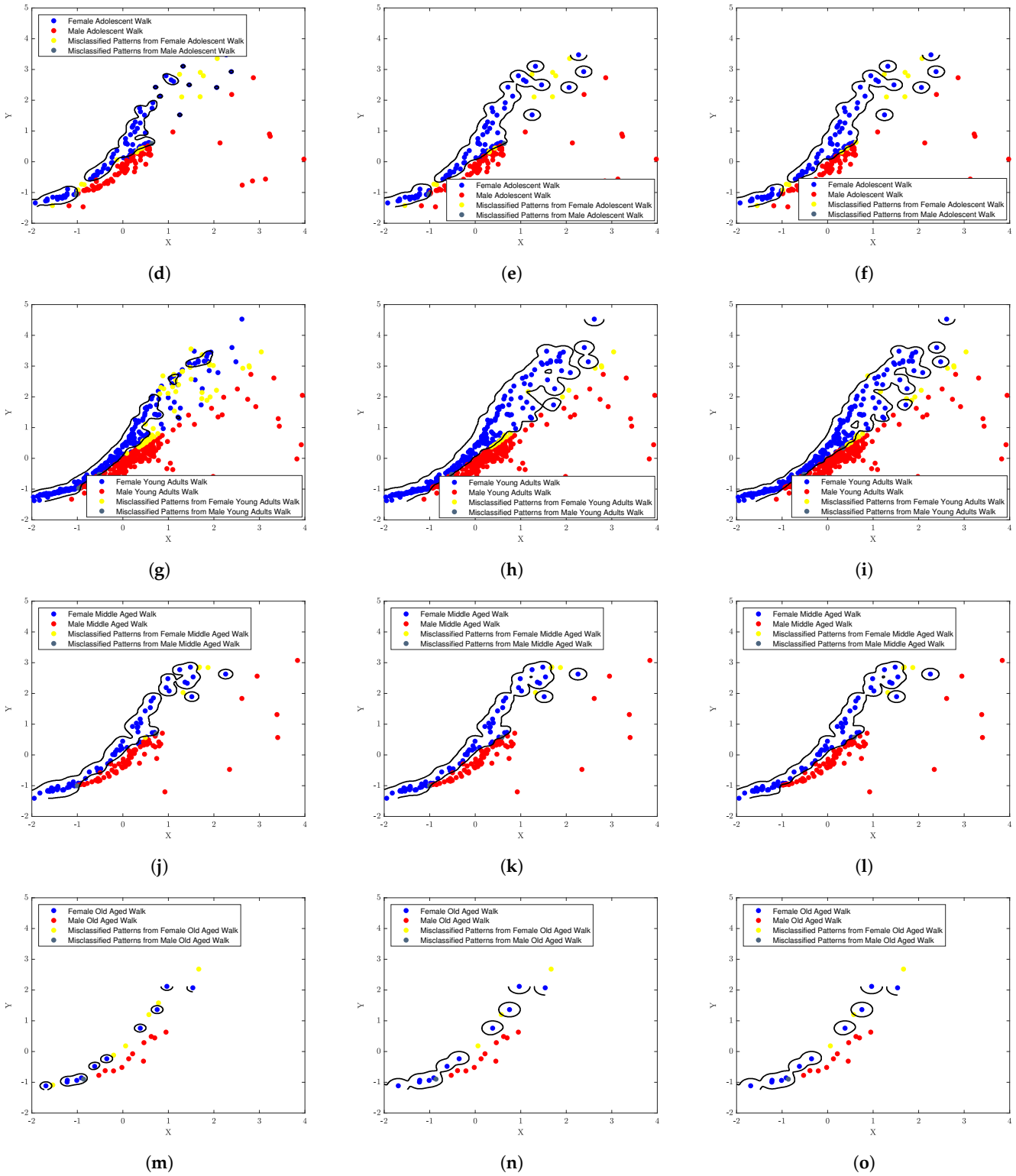

Figure 8. SVM decision boundaries with a Gaussian kernel for classifying walking trajectories across five demographic groups and both genders. Subfigures (**a**–**c**) show results for children, (**d**–**f**) adolescents, (**g**–**i**) young adults, (**j**–**l**) middle-aged adults, and (**m**–**o**) older adults. Within each group, the regularisation parameter is varied as $C = 0.1$ in in (**a**,**d**,**g**,**j**,**m**), $C = 1$ in (**b**,**e**,**h**,**k**,**n**), and $C = 10$ in (**c**,**f**,**i**,**l**,**o**), with the kernel width fixed at $\sigma = 0.1$.

In Figure 8g–i, the decision boundaries exhibit a similar progression. As C increases, the model adapts to finer complexities of the data points. However, the tighter clustering of data in the adult group compared to the children's group suggests that adult gait characteristics are more defined, likely due to a combination of physical maturity, including less relative variation in height and leg length, and adjustments in motor control mechanisms. These factors likely result in a more stable and less variable gait, which requires less aggressive tuning for optimal boundary creation. Figure 8g with $C = 0.1$ illustrates a wide decision boundary, which creates a balance between classification and generalisation. Meanwhile, Figure 8i, where $C = 10$, defines the classes with increased precision but at a potential risk of misclassification due to overfitting.

Figure 8j–l depict a clear decision boundary as C increases, similar to previous age groups. However, the scattered distribution of data points and their spatial separation indicate a greater variability in gait patterns among older adults, possibly due to age-related physical changes. Obviously, Figure 8m,o reveal a complex decision boundary that seems adept at detecting variations in gait, which suggests that higher C values might be beneficial in scenarios with significant class overlap or complex patterns.

Similarly, the series of plots shown in Figures 9 and 10 demonstrate the use of the SVM classifier with a Gaussian kernel under different configurations of σ and C, along with the CA methodology. The results indicate that this combination significantly improves the classification of nonlinear gait dynamics across pairwise age group comparisons for a single gender (either male or female), which shows the effectiveness of the approach in distinguishing gait patterns.

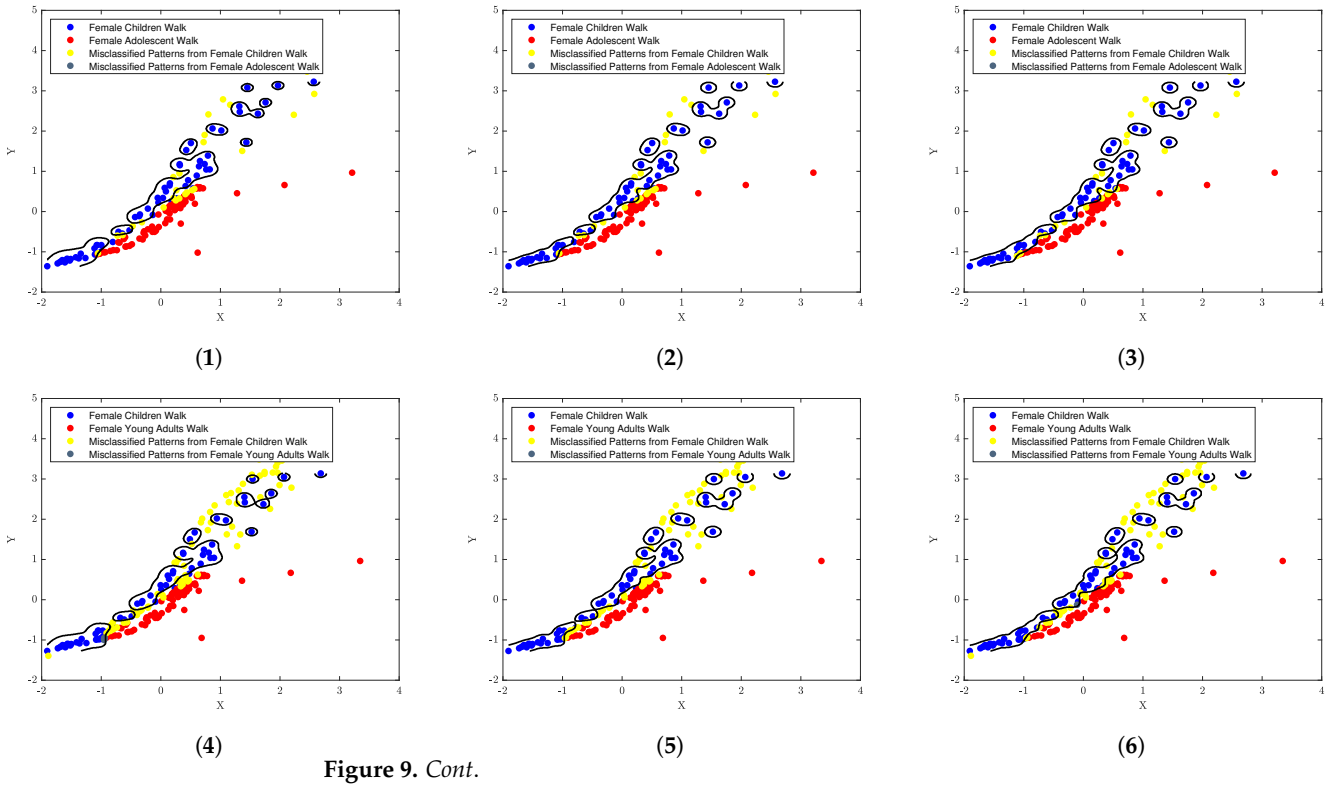

Figure 9. *Cont.*

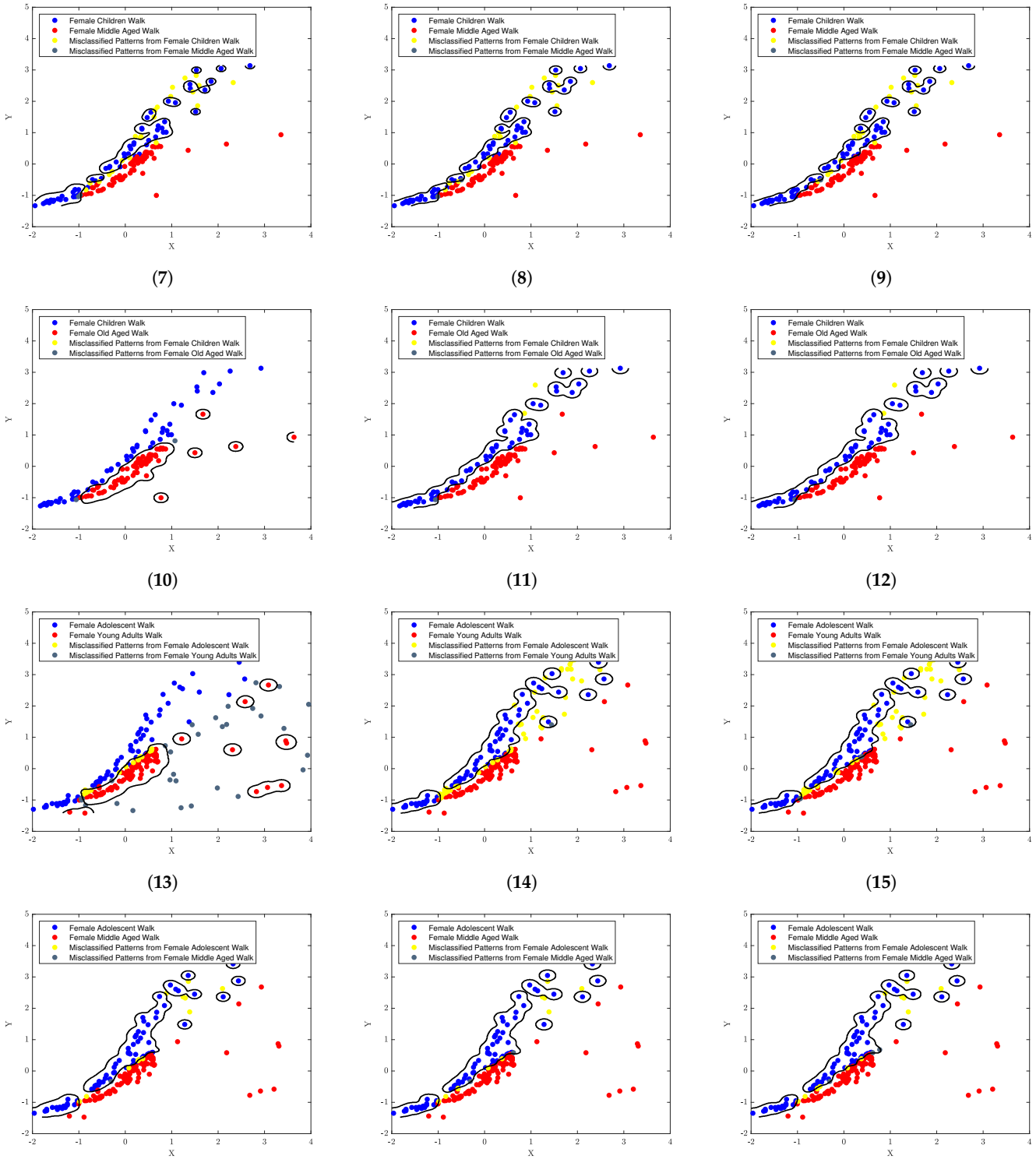

Figure 9. *Cont.*

https://doi.org/10.3390/math14010177

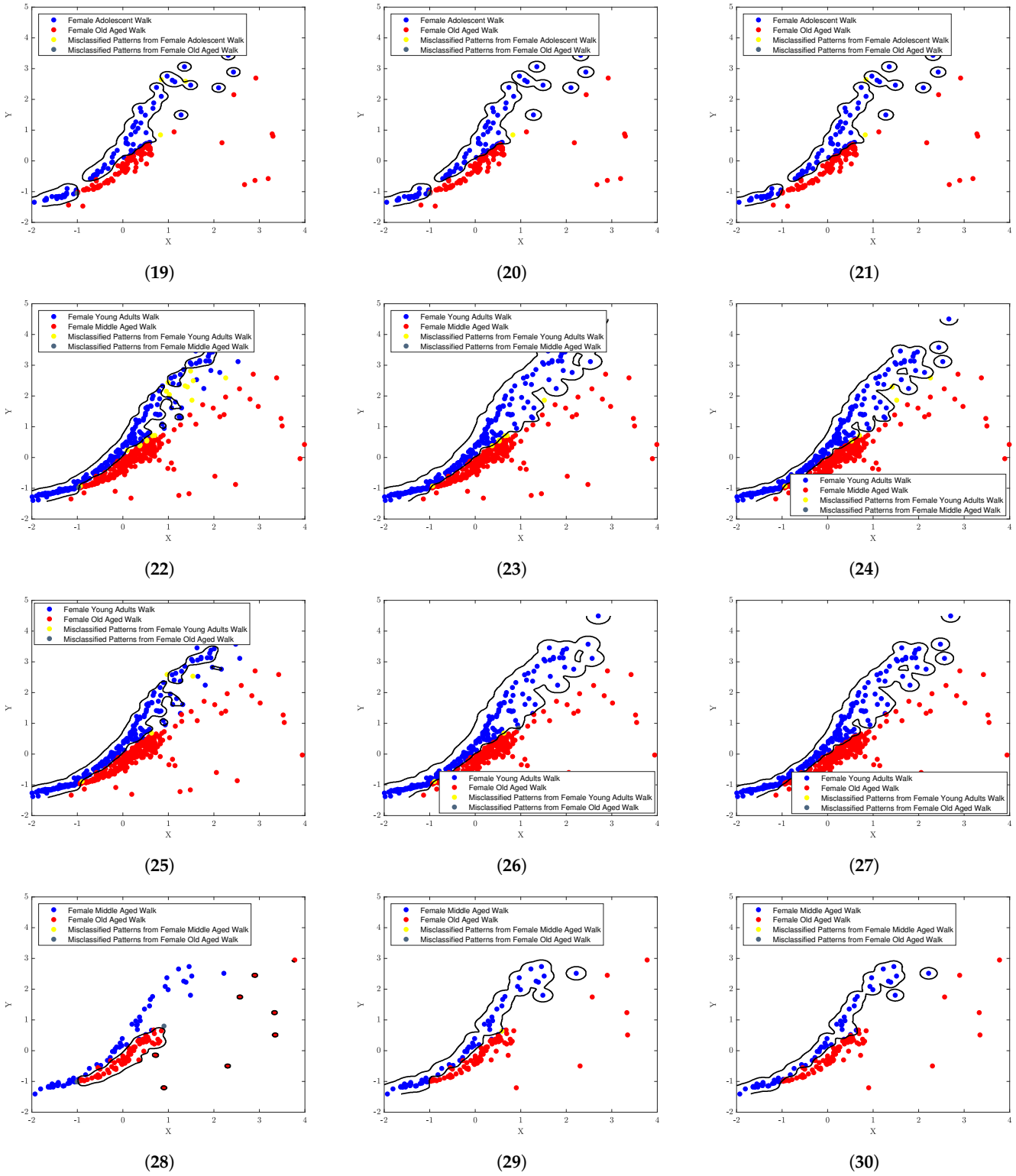

Figure 9. SVM decision boundaries with a Gaussian kernel for classifying walking trajectories of female participants across ten age categories. Each row corresponds to one age category, from children (row 1, subfigures (**1**–**3**)) to the oldest group (row 10, subfigures (**28**–**30**)). Within each row, the columns show the effect of varying the regularisation parameter C: left column $C = 0.1$, middle column $C = 1$, and right column $C = 10$. The Gaussian kernel width is fixed at $\sigma = 0.1$ for all subfigures.

https://doi.org/10.3390/math14010177

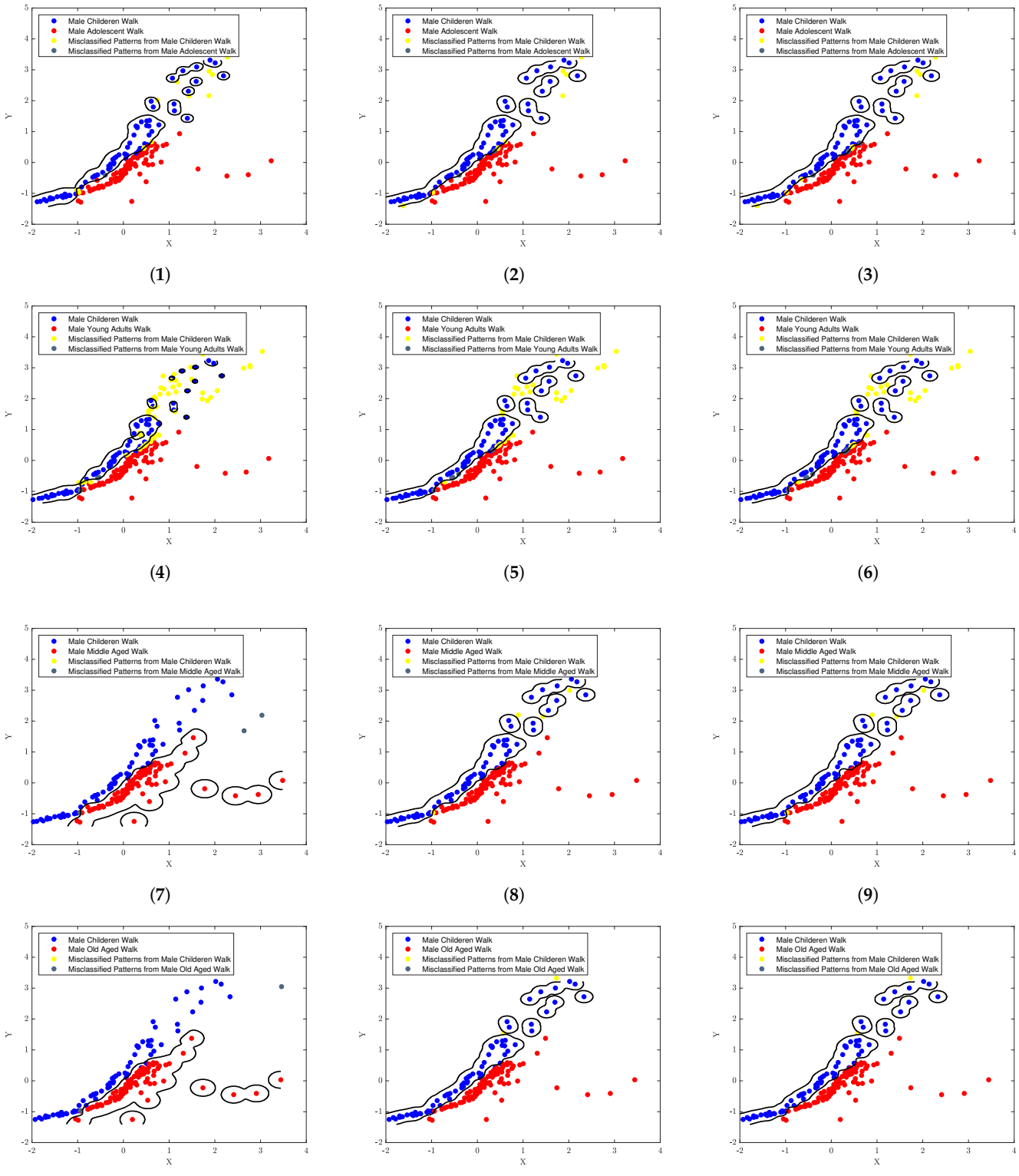

Figure 10. *Cont.*

https://doi.org/10.3390/math14010177

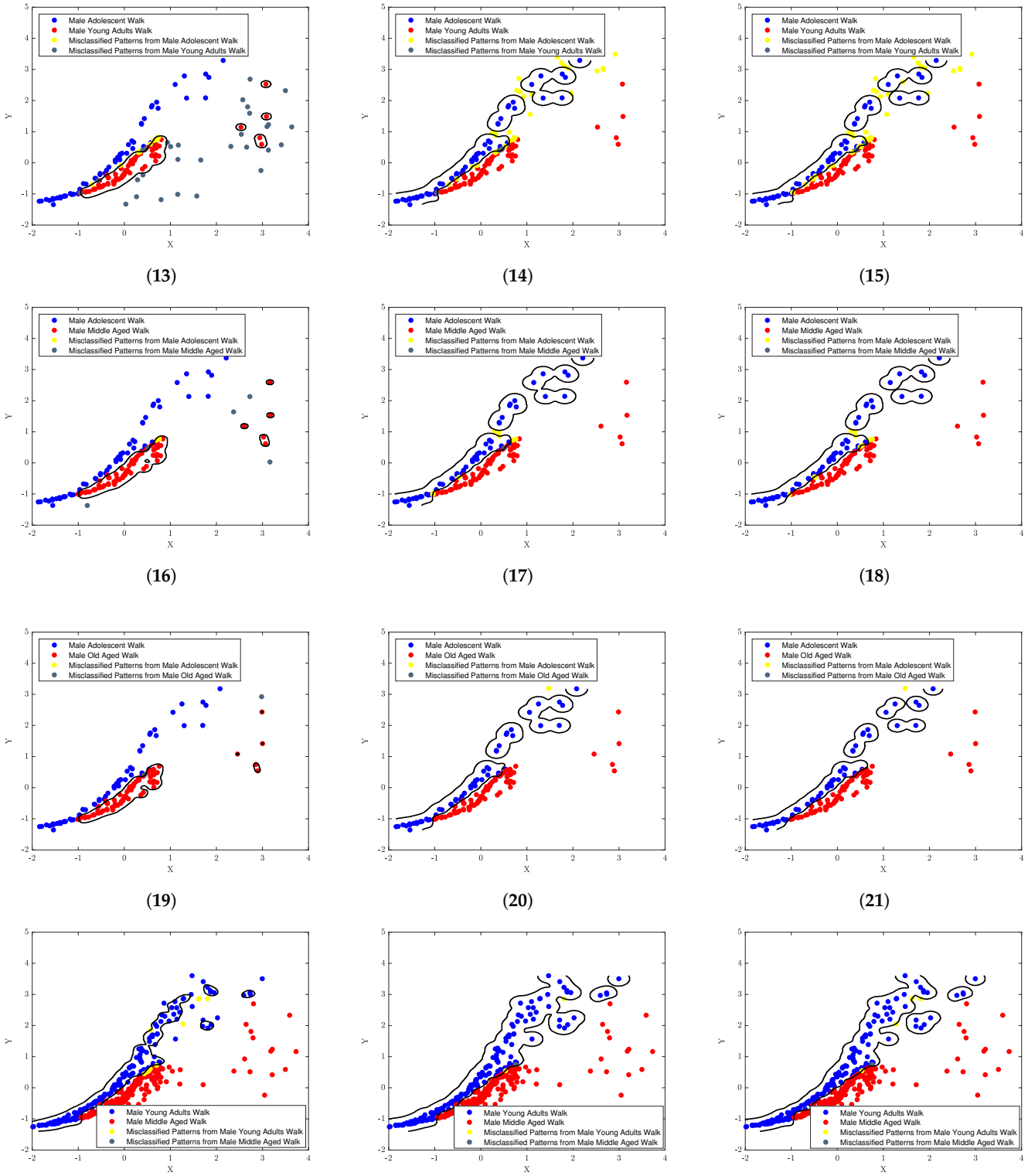

Figure 10. *Cont.*

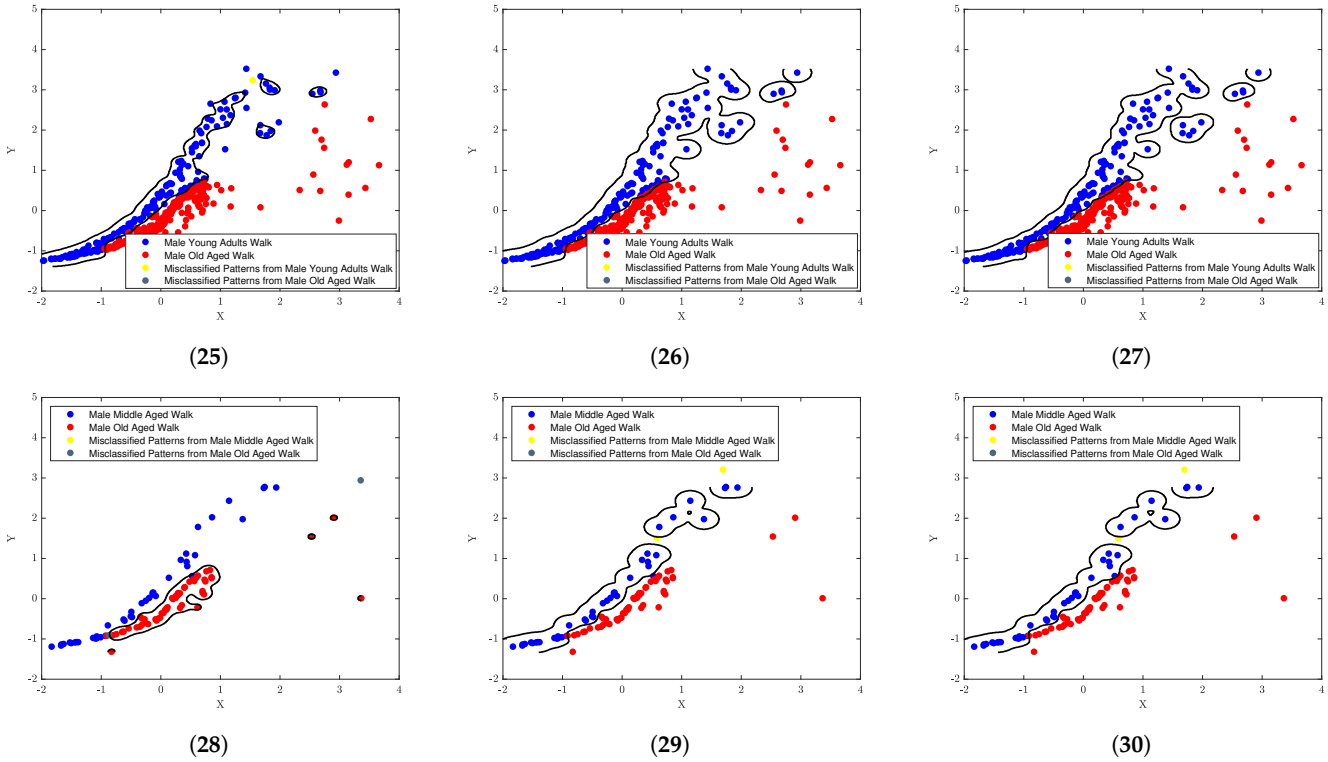

Figure 10. SVM decision boundaries with a Gaussian kernel for classifying walking trajectories of male participants across ten age categories. Each row corresponds to one age category, from children (row 1, subfigures (**1**–**3**)) to the oldest group (row 10, subfigures (**28**–**30**)). Within each row, the columns show the effect of varying the regularisation parameter C: left column $C = 0.1$, middle column $C = 1$, and right column $C = 10$. The Gaussian kernel width is fixed at $\sigma = 0.1$ for all subfigures.

In addition, we evaluated the performance of SVM classifiers in distinguishing gait patterns across different demographic groups for the three experiments we ran by monitoring the area under the ROC curve (AROC) (shown in Figures 11, 12 and 13, respectively), which provides a single numeric measure of classification ability. Higher AROC corresponds to better separation between classes, which allows us to examine how gender- or age-specific gait differences are captured and how the model responds to different regularisation parameters C.

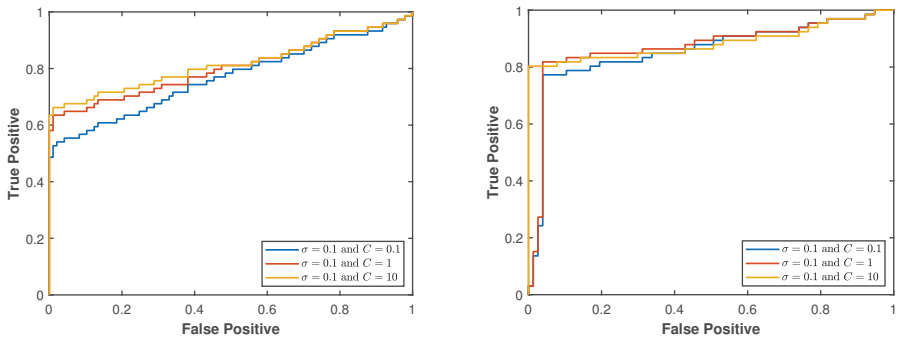

Figure 11. *Cont.*

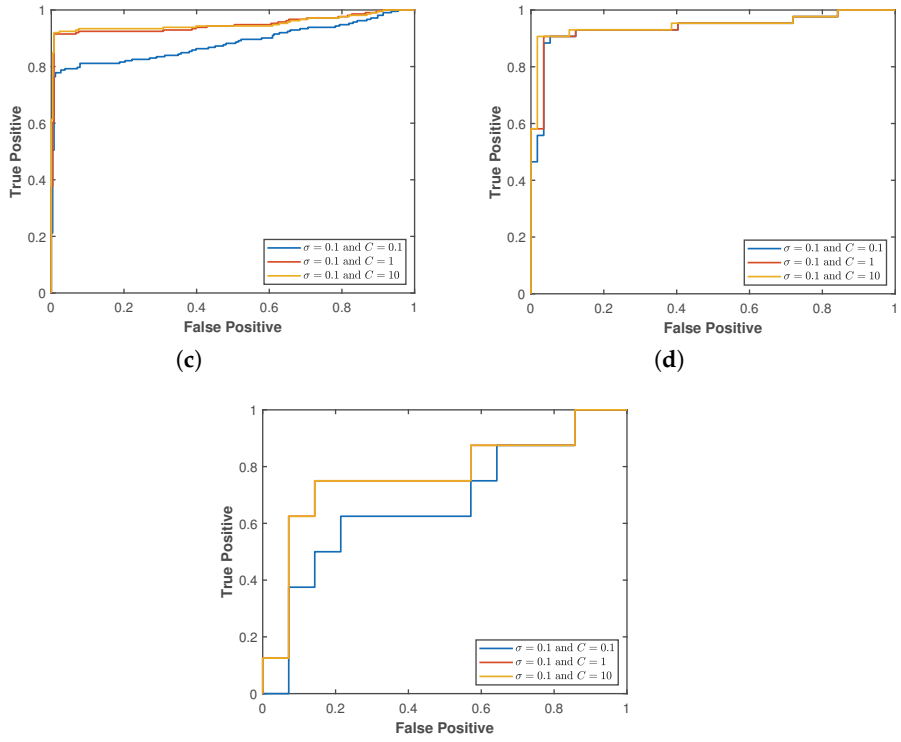

Figure 11. ROC curves comparing classification performance of walking patterns between male and female participants within each demographic group. Subplots show: (**a**) Children, (**b**) Adolescents, (**c**) Young Adults, (**d**) Middle Aged, and (**e**) Older Adults. Each curve represents a different regularisation parameter C (0.1, 1, 10) with fixed $\sigma = 0.1$, showing the effect of hyperparameter variation on the model's ability to distinguish gender-specific gait patterns. Note: In subplot (**e**), the red curve corresponding to $C = 1$ overlaps with the curve for $C = 10$, which makes it visually indistinguishable.

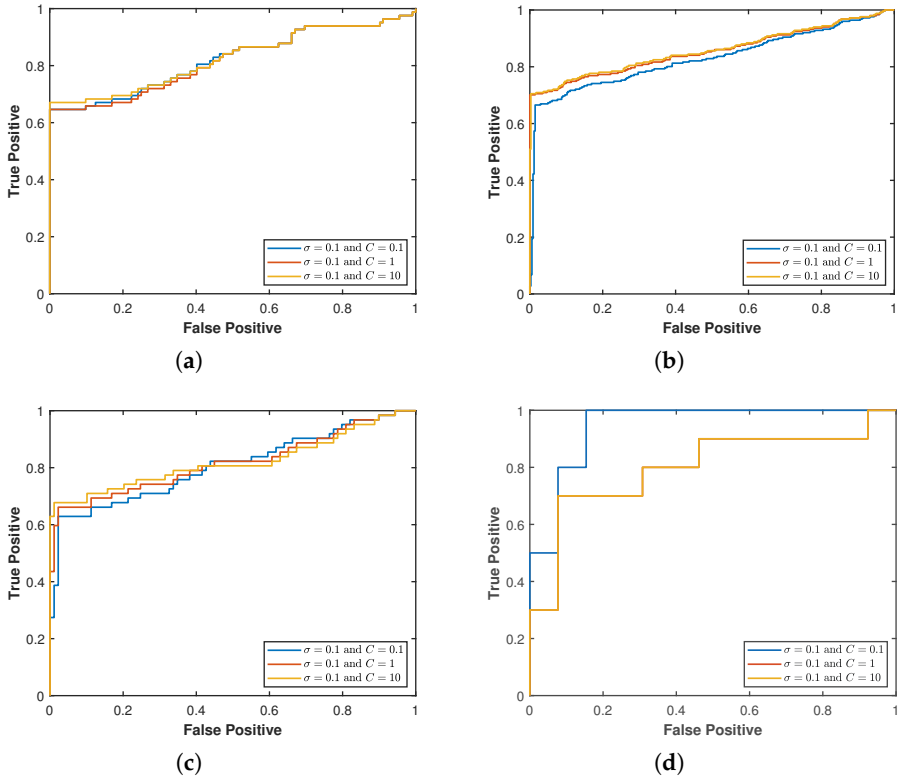

Figure 12. *Cont.*

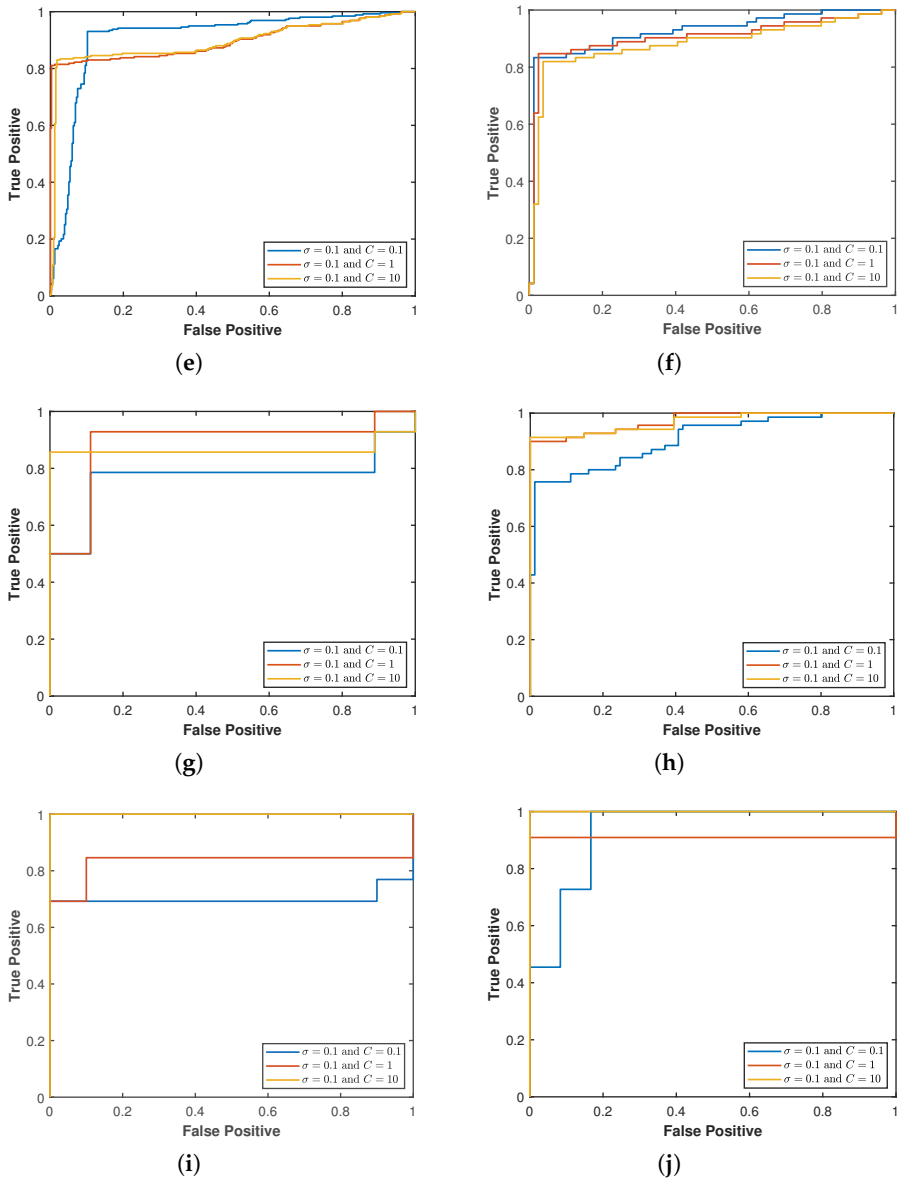

Figure 12. ROC curves showing the performance of the classification models in distinguishing walking patterns between different female demographic groups. Each subplot compares a specific pair of groups: (**a**) Children vs. Adolescents, (**b**) Children vs. Young Adults, (**c**) Children vs. Middle Aged, (**d**) Children vs. Older Adults, (**e**) Adolescents vs. Young Adults, (**f**) Adolescents vs. Middle Aged, (**g**) Adolescents vs. Older Adults, (**h**) Young Adults vs. Middle Aged, (**i**) Young Adults vs. Older Adults, and (**j**) Middle Aged vs. Older Adults. Each curve within a subplot represents a different regularisation parameter C (0.1, 1, 10) with fixed $\sigma = 0.1$, illustrating how model performance varies across hyperparameter settings and age-group comparisons. Note: In subplot (**d**), the red curve corresponding to $C = 1$ overlaps with the curve for $C = 10$, which makes it visually indistinguishable.

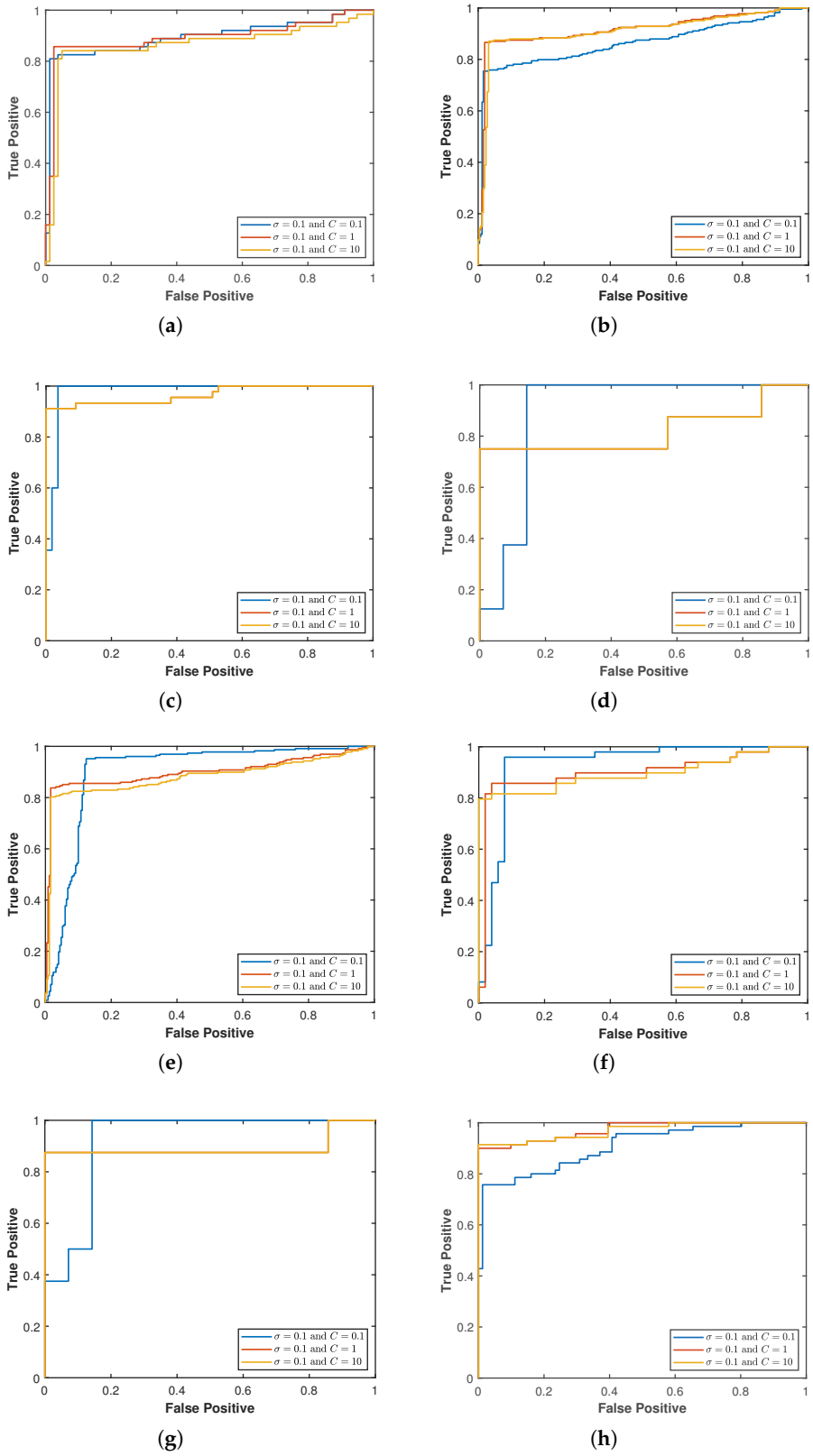

Figure 13. *Cont.*

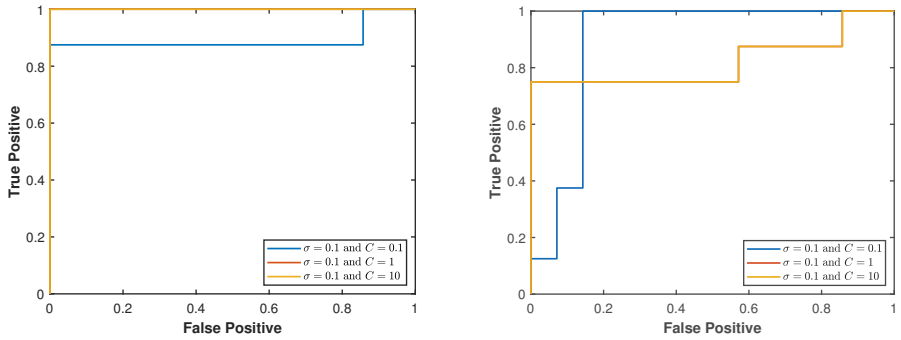

Figure 13. ROC curves showing the performance of the classification models in distinguishing walking patterns between different male demographic groups. Each subplot compares a specific pair of groups: (**a**) Children vs. Adolescents, (**b**) Children vs. Young Adults, (**c**) Children vs. Middle Aged, (**d**) Children vs. Older Adults, (**e**) Adolescents vs. Young Adults, (**f**) Adolescents vs. Middle Aged, (**g**) Adolescents vs. Older Adults, (**h**) Young Adults vs. Middle Aged, (**i**) Young Adults vs. Older Adults, and (**j**) Middle Aged vs. Older Adults. Each curve within a subplot represents a different regularisation parameter C (0.1, 1, 10) with fixed $\sigma = 0.1$, illustrating how model performance varies across hyperparameter settings and age-group comparisons. Note: In subplots (**c**,**d**,**g**,**i**,**j**), the red curve corresponding to $C = 1$ overlaps with the curve for $C = 10$, which makes it visually indistinguishable.

The ability of the classifier to distinguish male and female walking patterns generally improves with increasing C. For instance, in young adults ($\mathbf{x}_{\text{fm3}}$), AROC rises from 88% at $C = 0.1$ to 95% at $C = 10$, highlighting the strong influence of hyperparameter choice. Children ($\mathbf{x}_{\text{fm1}}$) and older adults ($\mathbf{x}_{\text{fm5}}$) exhibit lower AROC, ranging from 77–82% and 67–77%, respectively, indicating weaker gender differences or higher gait variability. The approximate standard deviation of AROC across C for each group is about 3–4% for young adults, reflecting the importance of tuning C, while older adults show a slightly higher spread of 5–6%, suggesting consistently lower classification performance. Figure 14 summarises the model's ability to separate young and middle-aged adults more reliably, whereas children and older adults remain more challenging for classification.

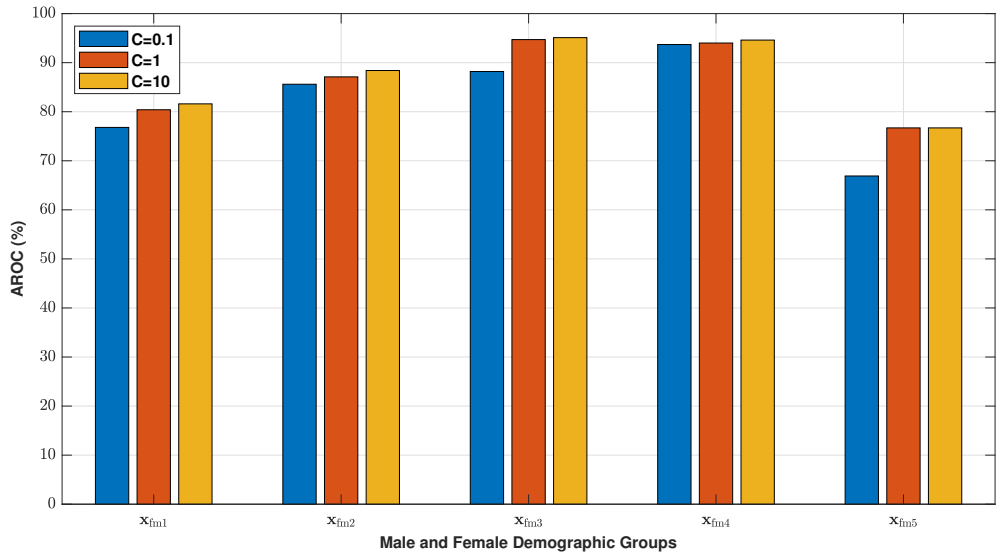

Figure 14. Gender classification performance using SVM, whose kernel width is fixed at $\sigma = 0.1$ and whose regularisation values are $C = 0.1, 1, 10$. Lines represent $\mathbf{x}_{\text{fm1}}$ to $\mathbf{x}_{\text{fm5}}$, and bars report AROC percentages describing the model's ability to separate male and female gait in each demographic group.

Classification across female age groups shows greater variability. Certain pairs, such as Young Adults vs. Middle Aged ($\mathbf{x}_{f8}$), achieve 91–97%, while others, like Young Adults vs. Older Adults ($\mathbf{x}_{f9}$), range from 70 to 100%. Higher C generally improves performance, but some pairs ($\mathbf{x}_{f4}$) drop from 95% to 80%, showing sensitivity to hyperparameters. The standard deviation across C values ranges from 2% to 12%, reflecting that some age-group comparisons are easier to classify than others due to subtle gait differences. Figure 15 shows that the classifier performs reasonably well for female participants, but its confidence depends on how distinctive the gait patterns are between age groups.

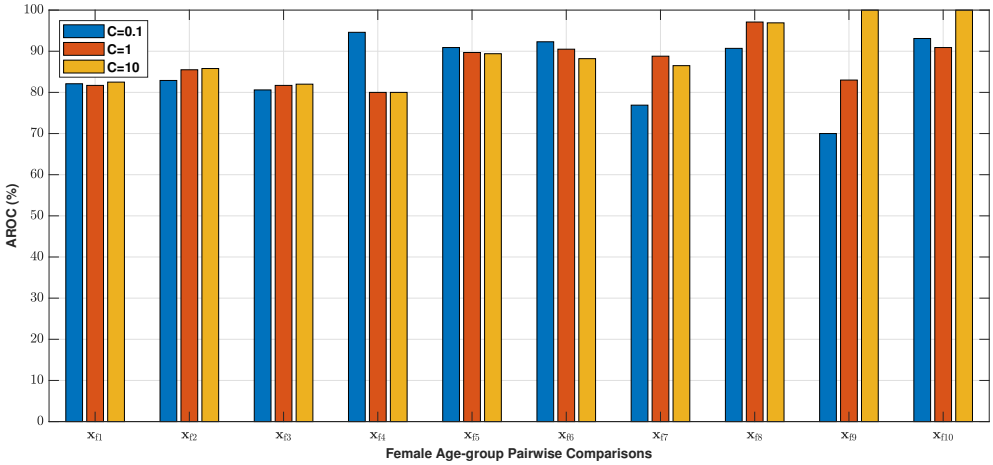

Figure 15. Pairwise female age-group comparisons $\mathbf{x}_{f1}$ to $\mathbf{x}_{f10}$ using SVM with fixed $\sigma = 0.1$ and $C = 0.1, 1, 10$. AROC percentages in each comparison measure the sharpness of age-separable decision boundaries in female gait across demographic distances.

For male participants, the classifier reaches AROC values mostly between 86% and 100%. Young adults ($\mathbf{x}_{m3}$) achieve scores around 98–97%, with very strong separation between male and female gait. A few demographics, such as $\mathbf{x}_{m1}$, drop slightly at higher C (from 89% to 86%), which means that too much regularisation can sometimes tighten the boundary more than needed and affect accuracy by a small margin. When we look at all ten age-group tests shown in Figure 16, the standard deviation of AROC sits roughly between 3–5%, which suggests that performance changes a moderate amount when either C or the age pair shifts. The runs where AROC climbs to 100% ($\mathbf{x}_{m9}$) tell us that for certain male demographics, their walking features are so distinct that the classifier draws a decision boundary with almost no overlap between the classes. These peak values confirm that the model is most dependable when male gait differences are clear and biologically or behaviourally pronounced across age groups.

Across all experiments, the classifier performs best on young and middle-aged adults, with AROC consistently above 90% for both male and female datasets. Children and older adults show lower performance (67–82%), reflecting more variable gait patterns. Standard deviation analysis across C shows how sensitive the model is to regularisation: higher std indicates significant performance changes with C, while lower values correspond to consistent but potentially lower accuracy. These results highlight the strengths and limitations of the classifier depending on demographic group and hyperparameter choice.

The classification performance of the three experiments was also complemented through examining the key metrics of the confusion matrix, such as precision, recall, F1-score, and accuracy. The results of the classification models derived from the confusion matrix metrics are tabulated in Tables A1–A3, which show the degree to which the SVM classifier generalises across various age groups and gender demographics. These results are further analysed through the lens of Figures 8–10, which provide deeper insights into

the behavior of the classifier with different parameter settings. The results for $\mathbf{x}_{\text{fm1}}$ (female and male children) illustrate that the decision boundary, shown in the first row of Figure 8, appears more flexible and adapts to variations in the feature space with a smaller σ and low C, as demonstrated by the mixed clustering of data points. However, it struggles with overfitting at $C = 0.1$ due to its sensitivity to noise. As C increases, the boundaries become smoother and more accurate, which better captures the true separation between classes. This improvement is reflected in better precision and recall at $C = 1$ and $C = 10$. However, as σ increases, the boundary loses definition, which indicates reduced specificity. Similarly, the third row of Figure 8, which corresponds to $\mathbf{x}_{\text{fm3}}$ (female and male young adults), illustrates that the classifier performs best with optimal σ and C. As σ increases, the boundaries become overly simplistic, which is evident at $\sigma = 10$, where data points from different classes overlap significantly. This can be interpreted as a reduction in both accuracy and specificity. Conversely, the last row of Figure 8 for $\mathbf{x}_{\text{fm5}}$ (female and male old-aged individuals) shows tight clustering at optimal configurations, which aligns with high precision and recall metrics. As σ increases, the decision boundaries become too simple, which leads to overfitting or underfitting. The same analysis follows for the results shown in both Tables A2 and A3 with respect to their visualisation shown in Figures 9 and 10.

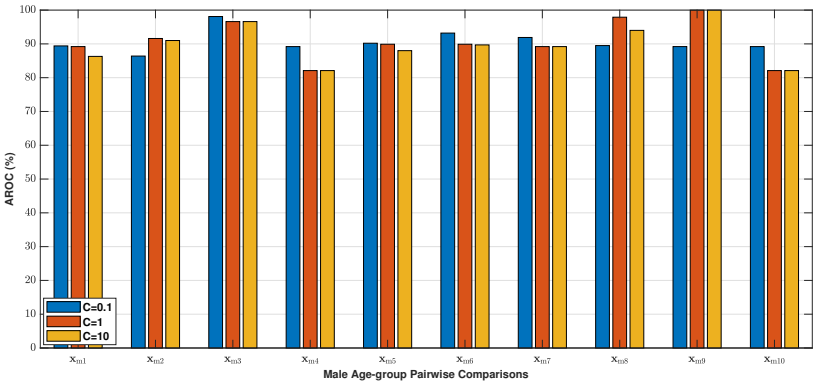

Figure 16. Gender classification performance for male participants using SVM, which uses a fixed $\sigma = 0.1$ and $C = 0.1, 1, 10$. Lines $\mathbf{x}_{\text{m1}}$ to $\mathbf{x}_{\text{m10}}$ show AROC percentages, whose values quantify how clearly male gait features form gender-separable decision boundaries under each regularisation strength.

Furthermore, Tables A1–A3 show how well the SVM classifies gait patterns using the CA features. Table A1 looks at male vs female overall, with accuracy from about 57% up to 97%, and generally high precision, recall, and F1-score. Table A2 focuses on female age group comparisons, showing strong accuracy mostly above 80% and consistently high F1-scores. Table A3 shows male age group comparisons, with similar trends and good overall performance. Across all tables, precision, recall, and F1-score show that the model correctly identifies classes while staying robust.

7. Conclusions

The effectiveness of the criticality analysis method in creating data-independent nonlinear representations was shown, with the aim of improving the detection of complex patterns in human gait dynamics across different demographic groups. The CA method was driven by a network of biologically-inspired chaotic mathematical models, controlled by the rate control of chaos, which is capable of controlling the chaotic exponential growth evolved over time and restoring stability to the system. This resulted in a network of controlled oscillators that produce a Self-Organised Critical system that is sensitive to the nonlinearities in the input data when perturbed. A visualisation of how dynamic trajectories are formed is provided, and the detection of any discrepancies introduced by the system is made obvious

without the need for further machine learning training. The classification of various gait patterns was validated using the SVM classifier with a Gaussian kernel function. This transformed the high-dimensional nonlinear gait patterns into a lower-dimensional representation space, where complex gait patterns can be identified efficiently. The combination of the CA methodology with supervised machine learning algorithms like the SVM is found to work really well, especially in capturing nonlinear relationships and enabling precise classification, allowing classification between genders and ages with high reliability.

Author Contributions: Conceptualisation, S.E.; methodology, S.E. and T.V.o.S.; validation, S.E.; formal analysis, S.E.; investigation, S.E.; data curation, H.D., J.C. and P.E.; writing—original draft preparation, S.E.; writing—review and editing, S.E. and T.V.o.S.; visualisation, S.E.; supervision, T.V.o.S. All authors have read and agreed to the published version of the manuscript.

Funding: The authors received no financial support for this research.

Data Availability Statement: The equation and generated data files for the Criticality Analysis (CA) model can be accessed publicly at https://doi.org/10.5281/zenodo.14960930.

Acknowledgments: The authors thank the Science Museum in London for facilitating data collection and sharing it with Oxford Brookes University for research.

Conflicts of Interest: The authors declare no conflicts of interest.

Appendix A

Table A1. Confusion matrix for gender-based (female and male) comparisons for each age group.

Performance	$\sigma = 0.1$			$\sigma = 1$			$\sigma = 10$		
	C = 0.1	**C = 1**	**C = 10**	**C = 0.1**	**C = 1**	**C = 10**	**C = 0.1**	**C = 1**	**C = 10**
					$\mathbf{x_{fm1}}$				
Precision	0.73	0.78	0.79	0.67	0.80	0.85	0.56	0.56	0.56
Recall	0.989	0.989	0.989	1	1	1	1	1	1
F1-Score	0.84	0.87	0.88	0.80	0.89	0.92	0.72	0.72	0.72
Accuracy (%)	78.94	83.62	84.79	73.09	86.54	90.64	56.72	56.72	56.72
					$\mathbf{x_{fm2}}$				
Precision	0.83	0.86	0.85	0.68	0.89	1	0.53	0.53	0.53
Recall	0.96	0.96	1	1	0.94	0.93	1	1	1
F1-Score	0.89	0.90	0.92	0.81	0.91	0.96	0.7	0.7	0.7
Accuracy (%)	87.41	89.51	90.90	74.83	90.9	96.5	53.84	53.84	53.84
					$\mathbf{x_{fm3}}$				
Precision	0.84	0.93	0.93	0.76	0.91	0.93	0.55	0.55	0.55
Recall	0.98	0.99	0.99	0.99	0.97	0.99	1	1	1
F1-Score	0.91	0.96	0.96	0.86	0.94	0.96	0.71	0.71	0.71
Accuracy (%)	89.53	95.81	96.02	82.42	93.93	95.81	55.64	55.64	55.64
					$\mathbf{x_{fm4}}$				
Precision	0.91	0.93	0.93	0.74	0.91	1	0.57	0.57	0.57
Recall	0.96	0.96	0.98	1	0.92	0.94	1	1	1
F1-Score	0.94	0.94	0.95	0.85	0.95	0.97	0.72	0.72	0.72
Accuracy (%)	93	94	95	80	95	97	57	57	57
					$\mathbf{x_{fm5}}$				
Precision	0.68	0.81	0.81	0.73	0.82	0.82	0.63	0.63	0.63
Recall	0.92	0.92	0.92	1	1	1	1	1	1
F1-Score	0.78	0.86	0.86	0.84	0.90	0.90	0.77	0.77	0.77
Accuracy (%)	68.18	81.81	81.81	77.27	86.36	86.36	63.63	63.63	63.63

Appendix B

Table A2. Confusion matrix for female-specific pairwise age group comparisons.

Performance	$\sigma = 0.1$			$\sigma = 1$			$\sigma = 10$		
	C = 0.1	**C = 1**	**C = 10**	**C = 0.1**	**C = 1**	**C = 10**	**C = 0.1**	**C = 1**	**C = 10**
				$\mathbf{x_{f1}}$					
Precision	0.79	0.79	0.80	0.65	0.78	0.79	0.57	0.57	0.57
Recall	1	1	1	1	1	1	1	1	1
F1-Score	0.88	0.88	0.89	0.78	0.87	0.88	0.73	0.73	0.73
Accuracy (%)	85.05	85.05	86.08	69.07	84.02	85.05	57.73	57.73	57.73
				$\mathbf{x_{f2}}$					
Precision	0.8	0.82	0.82	0.68	0.77	0.76	0.57	0.57	0.57
Recall	0.98	1	0.99	1	0.99	0.99	1	1	1
F1-Score	0.88	0.90	0.90	0.81	0.86	0.86	0.73	0.73	0.73
Accuracy (%)	85.01	87.37	87.37	73.06	82.65	81.64	57.74	57.74	57.74
				$\mathbf{x_{f3}}$					
Precision	0.78	0.79	0.80	0.71	0.83	0.83	0.58	0.58	0.58
Recall	0.97	0.97	0.98	1	0.99	0.99	1	1	1
F1-Score	0.87	0.87	0.88	0.83	0.90	0.90	0.74	0.74	0.74
Accuracy (%)	82.78	84.1	85.43	76.82	88.07	88.07	58.94	58.94	58.94
				$\mathbf{x_{f4}}$					
Precision	1	0.8	0.8	0.76	0.86	0.86	0.56	0.56	0.56
Recall	0.84	0.92	0.92	1	1	1	1	1	1
F1-Score	0.91	0.85	0.85	0.86	0.92	0.92	0.72	0.72	0.72
Accuracy (%)	91.3	82.6	82.6	82.6	91.3	91.3	56.52	56.52	56.52
				$\mathbf{x_{f5}}$					
Precision	0.94	0.87	0.88	0.72	0.94	0.96	0.58	0.56	0.56
Recall	0.89	0.99	0.98	0.99	0.95	0.98	1	1	1
F1-Score	0.91	0.93	0.92	0.83	0.94	0.97	0.73	0.72	0.72
Accuracy (%)	91.07	91.58	91.58	78.45	94.27	97.13	59.42	56.39	56.39
				$\mathbf{x_{f6}}$					
Precision	0.86	0.87	0.85	0.68	0.88	1	0.52	0.52	0.52
Recall	0.98	0.97	0.96	1	0.94	0.98	1	1	1
F1-Score	0.92	0.92	0.90	0.81	0.91	0.99	0.68	0.68	0.68
Accuracy (%)	91.39	91.39	89.4	75.49	90.72	99.33	52.31	52.31	52.31
				$\mathbf{x_{f7}}$					
Precision	0.72	0.88	0.81	0.56	0.63	1	0.39	0.39	0.39
Recall	0.88	0.88	1	1	0.77	1	1	1	1
F1-Score	0.8	0.88	0.9	0.72	0.7	1	0.56	0.56	0.56
Accuracy (%)	82.6	91.3	91.3	69.56	73.91	100	39.13	39.13	39.13
				$\mathbf{x_{f8}}$					
Precision	0.82	0.92	0.93	0.75	0.92	0.92	0.53	0.53	0.53
Recall	0.98	1	1	0.98	0.96	1	1	1	1
F1-Score	0.89	0.95	0.96	0.85	0.94	0.95	0.69	0.69	0.69
Accuracy (%)	88.07	95.36	96.02	82.11	94.03	95.36	53.64	53.64	53.64

Table A2. *Cont.*

Performance	$\sigma = 0.1$			$\sigma = 1$			$\sigma = 10$		
	C = 0.1	**C = 1**	**C = 10**	**C = 0.1**	**C = 1**	**C = 10**	**C = 0.1**	**C = 1**	**C = 10**
				$\mathbf{x_{f9}}$					
Precision	0.71	0.81	1	0.76	0.90	0.90	0.43	0.43	0.43
Recall	1	0.9	1	1	1	1	1	1	1
F1-Score	0.83	0.85	1	0.86	0.95	0.95	0.60	0.60	0.60
Accuracy (%)	82.6	86.95	100	86.95	95.65	95.65	43.47	43.47	43.47
				$\mathbf{x_{f10}}$					
Precision	1	0.92	1	0.75	0.90	0.92	1	0.52	0.52
Recall	0.83	1	1	1	0.83	1	0.5	1	1
F1-Score	0.90	0.96	1	0.85	0.86	0.96	0.66	0.68	0.68
Accuracy (%)	91.3	95.65	100	82.6	86.95	95.65	73.91	52.17	52.17

Appendix C

Table A3. Confusion matrix for male-specific pairwise age group comparisons.

Performance	$\sigma = 0.1$			$\sigma = 1$			$\sigma = 10$		
	C = 0.1	**C = 1**	**C = 10**	**C = 0.1**	**C = 1**	**C = 10**	**C = 0.1**	**C = 1**	**C = 10**
				$\mathbf{x_{m1}}$					
Precision	0.86	0.89	0.88	0.68	0.83	0.84	0.55	0.55	0.55
Recall	0.98	0.97	0.95	1	1	1	1	1	1
F1-Score	0.92	0.93	0.91	0.81	0.90	0.91	0.71	0.71	0.71
Accuracy (%)	90.9	92.3	90.2	74.12	88.81	89.51	55.94	55.94	55.94
				$\mathbf{x_{m2}}$					
Precision	0.81	0.89	0.89	0.63	0.86	0.85	0.53	0.53	0.53
Recall	0.98	0.98	0.96	1	0.99	1	1	1	1
F1-Score	0.89	0.93	0.93	0.77	0.92	0.92	0.69	0.69	0.69
Accuracy (%)	87.65	92.67	92.25	69.03	91.63	91.21	53.13	53.13	53.13
				$\mathbf{x_{m3}}$					
Precision	1	0.93	0.93	0.67	0.94	0.94	0.55	0.55	0.55
Recall	0.945	1	1	1	1	1	1	1	1
F1-Score	0.97	0.96	0.96	0.80	0.97	0.97	0.70	0.70	0.70
Accuracy (%)	97	96	96	73	97	97	55	55	55
				$\mathbf{x_{m4}}$					
Precision	1	0.87	0.87	0.82	1	1	0.63	0.63	0.63
Recall	0.85	1	1	1	0.92	0.92	1	1	1
F1-Score	0.92	0.93	0.93	0.80	0.97	0.97	0.77	0.77	0.77
Accuracy (%)	90.9	90.9	90.9	86.36	95.45	95.45	63.63	63.63	63.63
				$\mathbf{x_{m5}}$					
Precision	0.95	0.86	0.84	0.65	0.84	0.85	0.59	0.52	0.52
Recall	0.87	0.98	0.98	1	0.99	1	1	1	1
F1-Score	0.91	0.92	0.90	0.78	0.91	0.92	0.74	0.68	0.68
Accuracy (%)	91	91.42	89.74	71.96	89.95	91	63.8	52.3	52.3

Table A3. *Cont.*

Performance	$\sigma = 0.1$			$\sigma = 1$			$\sigma = 10$		
	C = 0.1	C = 1	C = 10	C = 0.1	C = 1	C = 10	C = 0.1	C = 1	C = 10
					x_{m6}				
Precision	0.95	0.84	0.83	0.62	0.81	0.82	0.98	0.51	0.51
Recall	0.90	0.98	1	1	0.98	1	0.96	1	1
F1-Score	0.92	0.90	0.91	0.76	0.89	0.90	0.97	0.67	0.67
Accuracy (%)	93	90	90	69	88	89	97	51	51
					x_{m7}				
Precision	1	0.93	0.93	0.82	1	0.93	0	0.63	0.63
Recall	0.85	1	1	1	1	1	0	1	1
F1-Score	0.92	0.96	0.96	0.90	1	0.96	0	0.77	0.77
Accuracy (%)	90.9	95.45	95.45	86.36	100	95.45	36.36	63.63	63.63
					x_{m8}				
Precision	0.83	0.96	0.90	0.70	0.87	0.77	0.51	0.51	0.51
Recall	1	0.98	0.98	1	1	1	1	1	1
F1-Score	0.91	0.97	0.94	0.82	0.93	0.87	0.67	0.67	0.67
Accuracy (%)	90	97	94	79	93	85	51	51	51
					x_{m9}				
Precision	0.93	1	1	0.87	1	0.93	0.63	0.63	0.63
Recall	1	1	1	1	0.92	1	1	1	1
F1-Score	0.96	1	1	0.93	0.96	0.96	0.77	0.77	0.77
Accuracy (%)	95.45	100	100	90.9	95.45	95.45	63.63	63.63	63.63
					x_{m10}				
Precision	1	0.87	0.87	0.82	1	1	1	0.63	0.63
Recall	0.85	1	1	1	0.92	1	0.78	1	1
F1-Score	0.92	0.93	0.93	0.90	0.96	1	0.88	0.77	0.77
Accuracy (%)	90.9	90.9	90.9	86.36	95.45	100	86.36	63.63	63.63

References

1. Bian, S.; Liu, M.; Zhou, B.; Lukowicz, P. The state-of-the-art sensing techniques in human activity recognition: A survey. *Sensors* **2022**, *22*, 4596. [CrossRef]
2. Baker, R. Gait analysis methods in rehabilitation. *J. Neuroeng. Rehabil.* **2006**, *3*, 4. [CrossRef]
3. Hausdorff, J.M. Gait variability: Methods, modeling and meaning. *J. Neuroeng. Rehabil.* **2005**, *2*, 19. [CrossRef]
4. Bouchrika, I. Gait Analysis and Recognition for Automated Visual Surveillance. Ph.D. Thesis, Department of Electronics and Computer Science, University of Southampton, Southampton, UK, 2008.
5. Dockstader, S.L.; Bergkessel, K.A.; Tekalp, A.M. Feature extraction for the analysis of gait and human motion. In Proceedings of the 2002 International Conference on Pattern Recognition, Quebec City, QC, Canada, 11–15 August 2002; Volume 1, pp. 5–8.
6. Figueiredo, J.; Santos, C.P.; Moreno, J.C. Automatic recognition of gait patterns in human motor disorders using machine learning: A review. *Med. Eng. Phys.* **2018**, *53*, 1–12. [CrossRef]
7. olde Scheper, T.V. Controlled bio-inspired self-organised criticality. *PLoS ONE* **2022**, *17*, e0260016. [CrossRef] [PubMed]
8. olde Scheper, T.V. Criticality Analysis: Bio-Inspired Nonlinear Data Representation. *Entropy* **2023**, *25*, 1660. [CrossRef]
9. Eltanani, S.; olde Scheper, T.V.; Muñoz-Balbontin, M.; Aldea, A.; Cossington, J.; Lawrie, S.; Villalpando-Carrion, S.; Adame, M.J.; Felgueres, D.; Martin, C.; et al. A Novel Criticality Analysis Method for Assessing Obesity Treatment Efficacy. *Appl. Sci.* **2023**, *13*, 13225. [CrossRef]
10. Eltanani, S.; olde Scheper, T.V.; Dawes, H. A Novel Criticality Analysis Technique for Detecting Dynamic Disturbances in Human Gait. *Computers* **2022**, *11*, 120. [CrossRef]
11. Wu, A.R. Human biomechanics perspective on robotics for gait assistance: Challenges and potential solutions. *Proc. Biol. Sci.* **2021**, *288*, 20211197. [CrossRef] [PubMed] [PubMed Central]
12. Townsend, M.A.; Seireg, A.A. Effect of Model Complexity and Gait Criteria on the Synthesis of Bipedal Locomotion. *IEEE Trans. Biomed. Eng.* **1973**, *BME-20*, 433–444. [CrossRef] [PubMed]

13. Thuilot, B.; Goswami, A.; Espiau, B. Bifurcation and chaos in a simple passive bipedal gait. In Proceedings of the International Conference on Robotics and Automation, Albuquerque, NM, USA, 20–25 April 1997; Volume 1, pp. 792–798. [CrossRef]
14. Morgado, M.L.; Morgado, L.F.; Silva, N.; Morais, R. Mathematical modelling of cylindrical electromagnetic vibration energy harvesters. *Int. J. Comput. Math.* **2014**, *92*, 101–109. [CrossRef]
15. Kurz, M.; Stergiou, N. An artificial neural network that utilizes hip joint actuations to control bifurcations and chaos in a passive dynamic bipedal walking model. *Biol. Cybern.* **2005**, *93*, 213–221. [CrossRef]
16. Pareja, J.L.; Martin, F.; Caceres, O.; Blanco, M.; Berral, F.J. P-11 Fibromyalgia: Looking for markers and the impact of a multidisciplinary treatment. *Br. J. Sports Med.* **2016**, *50*, A37–A38.
17. Stergiou, N.; Decker, L.M. Human movement variability, nonlinear dynamics, and pathology: Is there a connection? *Hum. Mov. Sci.* **2011**, *30*, 869–888. [CrossRef]
18. Ahn, J.; Hogan, N. Long-Range Correlations in Stride Intervals May Emerge from Non-Chaotic Walking Dynamics. *PLoS ONE* **2013**, *8*, e73239. [CrossRef]
19. Parakkal Unni, M.; Menon, P.P. Modelling and analysis of Parkinsonian gait. *Nonlinear Dyn.* **2023**, *111*, 753–769. [CrossRef]
20. Park, J.; Seeley, M.K.; Francom, D.; Reese, C.S.; Hopkins, J.T. Functional vs. traditional analysis in biomechanical gait data: An alternative statistical approach. *J. Hum. Kinet.* **2017**, *60*, 39–49. [CrossRef]
21. Prince, F.; Corriveau, H.; Hébert, R.; Winter, D.A. Gait in the elderly. *Gait Posture* **1997**, *5*, 128–135. [CrossRef]
22. Kang, H.G.; Dingwell, J.B. Separating the effects of age and walking speed on gait variability. *Gait Posture* **2008**, *27*, 572–577. [CrossRef]
23. Owings, T.M.; Grabiner, M.D. Step width variability, but not step length variability or step time variability, discriminates gait of healthy young and older adults during treadmill locomotion. *J. Biomech.* **2008**, *37*, 935–938. [CrossRef]
24. Hausdorff, J.M. Gait dynamics, fractals and falls: Finding meaning in the stride-to-stride fluctuations of human walking. *Hum. Mov. Sci.* **2007**, *26*, 555–589. [CrossRef] [PubMed]
25. Hamacher, D.; Liebl, D.; Hödl, C.; Heßler, V.; Kniewasser, C.K.; Thönnessen, T.; Zech, A. Gait stability and its influencing factors in older adults. *Front. Physiol.* **2019**, *9*, 1955. [CrossRef]
26. Tisser, R.; Robert, T.; Chabaud, P.; Bonnefoy, M.; Chèze, L. Elderly fallers enhance dynamic stability through anticipatory postural adjustments during a choice stepping reaction time. *Front. Hum. Neurosci.* **2016**, *10*, 613. [CrossRef] [PubMed]
27. van Kooten, D.; Hettinga, F.; Duffy, K.; Jackson, J.; Taylor, M.J. Are there associations with age and sex in walking stability in healthy older adults? *Gait Posture* **2018**, *60*, 65–70. [CrossRef]
28. Bizovska, L.; Svoboda, Z.; Kutilek, P.; Janura, M.; Gaba, A.; Kovacikova, Z. Variability of centre of pressure movement during gait in young and middle-aged women. *Gait Posture* **2014**, *40*, 399–402. [CrossRef]
29. Crenshaw, J.R.; Bernhardt, K.A.; Achenbach, S.J.; Atkinson, E.J.; Khosla, S.; Kaufman, K.R.; Amin, S. The circumstances, orientations, and impact locations of falls in community-dwelling older women. *Arch. Gerontol. Geriatr.* **2017**, *73*, 240–247. [CrossRef]
30. Rowe, E.; Beauchamp, M.K.; Wilson, J.A. Age and sex differences in normative gait patterns. *Gait Posture* **2021**, *88*, 109–115. [CrossRef]
31. Hughes-Oliver, C.N.; Srinivasan, D.; Schmitt, D.; Queen, R.M. Gender and limb differences in temporal gait parameters and gait variability in ankle osteoarthritis. *Gait Posture* **2018**, 65, 228–233. [CrossRef] [PubMed]
32. Deutsch, A.; Dormann, S. *Mathematical Modeling of Biological Pattern Formation*; Birkhäuser: Boston, MA, USA, 2005; pp. 45–56.
33. Beek, P.J.; Peper, C.E.; Stegeman, D.F. Dynamical models of movement coordination. *Hum. Mov. Sci.* **1995**, *14*, 573–608. [CrossRef]
34. van Emmerik, R.E.; van Wegen, E.E. On variability and stability in human movement. *J. Appl. Biomech.* **2000**, *16*, 394–406. [CrossRef]
35. Taga, G. A model of the neuro-musculo-skeletal system for human locomotion: I. Emergence of basic gait. *Biol. Cybern.* **1995**, *73*, 97–111. [CrossRef]
36. Dingwell, J.B.; Cusumano, J.P. Nonlinear time series analysis of normal and pathological human walking. *Chaos Interdiscip. J. Nonlinear Sci.* **2000**, *10*, 848–863. [CrossRef]
37. Piorek, M.; Josinski, H.; Michalczuk, A.; Switonski, A.; Szczesna, A. Quaternions and joint angles in an analysis of local stability of gait for different variants of walking speed and treadmill slope. *Inf. Sci.* **2017**, *384*, 263–280. [CrossRef]
38. Ott, E. *Chaos in Dynamical Systems*; Cambridge University Press: Cambridge, UK, 2002.
39. Close, C.M.; Frederick, D.K.; Newell, J.C. *Modeling and Analysis of Dynamic Systems*; John Wiley and Sons: Hoboken, NJ, USA, 2001.
40. Gorley, P.N.; Horley, P.P.; Tomchuk, P.M. Trajectory tracing—A new method of studying the evolution of states of dynamic systems. *Tech. Phys. Lett.* **1999**, *25*, 7–9. [CrossRef]
41. Thelen, E.; Smith, L.B. *Dynamic Systems Theories*; John Wiley and Sons: Hoboken, NJ, USA, 1998.
42. Berry, H. Chaos in a Bienzymatic Cyclic Model with Two Autocatalytic Loops. *Chaos Solitons Fractals* **2003**, *18*, 1001–1014. [CrossRef]
43. Eltanani, S. The Criticality Analysis for Berry Model—Equation File and Its Generated Data. *Zenodo* **2025**. [CrossRef]

44. Esser, P.; Dawes, H.; Collett, J.; Howells, K. IMU: Inertial Sensing of Vertical CoM Movement. *J. Biomech.* **2009**, *42*, 1578–1581. [CrossRef] [PubMed]
45. Esser, P.; Dawes, H.; Collett, J.; Feltham, M.G.; Howells, K. Assessment of spatio-temporal gait parameters using inertial measurement units in neurological populations. *Gait Posture* **2011**, *34*, 558–560. [CrossRef] [PubMed]